

Geochemical characterization of the Krishna-Godavari and Mahanadi offshore basin (Bay of Bengal) sediments: A comparative study of provenance

A. Mazumdar^{1*}, M. Kocherla¹, Mary Ann Carvalho¹, A. Peketi¹, R. K. Joshi², P. Mahalaxmi¹, H. M. Joao¹, R. Jisha³

¹*Geological Oceanography,
CSIR-National Institute of Oceanography, Dona Paula, Goa-403004, India*
*for correspondence: maninda@nio.org

²*Geological Survey of India
Kolkata-700 091, India*

³*Sreelayam Kongatta Pathayakunnu (PO)
Thalalassery, Kannur District
Kerala -670 691*

Abstract

The Krishna-Godavari and Mahanadi rivers drain the east coast of India and deposit the sediment load into the Krishna-Godavari and Mahanadi offshore basins along the western margin of the Bay of Bengal. Here we report the bulk major, trace and rare earth element (REE) compositions and clay mineralogy of the fine grained sediments from the cores collected on board *JOIDES Resolution* and *Marion Dufresne* as part of India's gas hydrate program. The geochemical composition and clay mineralogy of sediments have been used to constrain the provenance. The results show that the Mahanadi sediments are primarily derived from the felsic rocks belonging to the late Archean-early Proterozoic Peninsular Gneissic Complexes, whereas the Krishna-Godavari sediments are derived from the mixing of late Archean-early Proterozoic Peninsular Gneissic Complexes and late Cretaceous Deccan basalt sources. This paper presents the first comparative analysis of provenance of the Krishna-Godavari (K-G) and Mahanadi offshore basin sediments. The sediment geochemistry enables distinction of specific contributing sources, which could potentially be related to modern climatic and geomorphological conditions. The present study could also provide the opportunity for high resolution paleoclimatic analysis using clay mineralogical contents and weathering indices (Haughton et al., 1991).

Keywords: Krishna-Godavari basin, Mahanadi Basin, provenance, clay mineralogy, Deccan basalt, Peninsular Gneissic complex.

1. Introduction

Geochemical and mineralogical compositions can be used to evaluate the provenance of marine sediments and sedimentary rocks (Wronkiewicz and Condie, 1987; Cullers, 1994; Cullers, 1995; Fralick and Kronberg, 1997; Young and Nesbitt; 1998; Weltje and Eynatten, 2004; Wei et al., 2003, 2004; Whitemore et al., 2004; Hongxia et al., 2007; Roy et al., 2007; Perri et al., 2011a, b, 2012, 2013). Homogenous, fine grained sediments composed of clay and silt size particles are inferred to represent the average composition of the source rocks (Rudnick and Gao, 2003; Weltje and Eynatten, 2004). Using major/trace element composition and clay mineralogical assemblages, marine sediments may be linked to different source rocks (Nesbitt and Young, 1989). The chemical weathering of the source rock is primarily carried out by the carbonic and organic acids in percolating ground water (Huang and Keller, 1970; Berner, 1992; Welch and Ullman, 1993). Several factors such as grain size, adsorption of ions by clays, mobilization of elements during diagenesis, climate, bulk composition of the source terrain, and tectonic setting influence the chemical composition of marine sediments (Bhatia and Crook, 1986; Wronkiewicz and Condie, 1989; Cullers.1994; Nagender Nath et al., 2000). Thorium, Zr, Hf, Nb, Sc, Cr, Ni, V, Ba, Rb and rare earth elements (REE) are thought to be the most suitable components for provenance determination because of their refractory nature and very low mobility during weathering and diagenetic processes (Taylor and McLennan, 1985). These elements are incorporated into the clastic sediments during weathering and transportation with little fractionation and are expected to reflect the signature of the parent material (Taylor and McLennan, 1985; McLennan et al., 1993; McLennan, 2001). The relative distribution of immobile elements can help to infer the relative contribution of silcic and mafic source rocks in the sediments. High ratios of La or Th to Co, Sc, Cr and Ni suggest derivation from silicic sources whereas lower ratios indicate basic provenance (Cullers, 2002). Rare earth element concentrations in marine sediments are believed to reflect the REE distribution pattern of the source material (Ronov et al., 1974; Taylor and McLennan, 1985; Cullers et al, 1987; Condie, 1991) and may help to discriminate between mafic and felsic source rocks using the Eu anomaly, and C1-chondrite normalized Σ LREE/ Σ HREE and La/Yb ratios (Cullers and Graf, 1983; Taylor and McLennan,1985; McLennan,1989).

In the present study major, trace and REE data of three cores (NGHP-EXP1-3B, 5C and 18A) collected on-board *JOIDES Resolution* off the Krishna-Godavari and Mahanadi basins in the Bay of Bengal are presented and discussed in terms of the relative contributions of mafic and silicic source detritus from peninsular India. In addition, we present clay mineralogical data from two cores,

MD161-8 and 19 collected on board the *Marion Dufresne* off the Krishna-Godavari and Mahanadi basins, respectively.

2. Geology

2.1 Krishna-Godavari basin

The Krishna-Godavari basin (K-G basin) is a pericratonic rift basin (Fig. 1) with onshore and offshore extensions. The rift basin extends offshore along the eastern continental margin of India (ECMI). The K-G basin covers an area of 28,000 km² onshore and 145,000 km² offshore (Rao, 2001; Bastia, 2007). Geographically, it lies between Kakinada in the northeast and Ongole in the southwest of Andhra Pradesh. The ECMI represents a passive continental margin that evolved through the break-up of the eastern Gondwana landmass ~130 My ago when India separated from East Antarctica (Ramana et al., 1994). The basin is characterized by en echelon type horst and graben-like structures (Rao and Mani, 1993; Rao, 2001; Gupta, 2006). The initial rifting and drifting phase during the Cretaceous resulted in extensive deposition of fluvio-lacustrine sediments throughout the basin. A sediment thickness of 3-5 km in the onshore region and around 8 km in the offshore region have been reported by Bastia (2007) and Prabhakar and Zutshi (1993). A south-easterly tilt in the late Cretaceous resulted in an extensive marine transgression which led to deposition of the Ragavapuram shale (Sastri et al., 1973). The Ragavapuram shale is overlain successively by the Razole Formation, Palakollu Shale, Vadaparru shale, Narsapur claystone, Ravva Formation and Godavari clay. The Godavari Clay ranges in age from mid Pliocene to Holocene.

The Krishna and Godavari rivers are the main drainage systems through the source rocks of the Krishna-Godavari basin. The Krishna river catchment lies between 13° - 19°30' N and 73°23' - 80°30' E and its area is 258,948 km². The river originates in the Western Ghats at an elevation of 1337 m above mean sea level. Estimated annual sediment flux is 67.72x10⁶ ton yr⁻¹ (Ramesh and Subramanian, 1988). The Bhima and Tungabhadra are the major tributaries whereas Ghataprabha and Malaprabha are the minor tributaries. Except in the upper reaches, semi-arid conditions prevail in most of the catchment area. Most of the catchment area (80%) is occupied by late Archaean and early Proterozoic crystalline rocks. Tertiary Deccan traps (basalt) and recent sediments outcrop locally (20%) (Ramesh and Subramanian, 1988).

The Godavari catchment (16-18°N and 75-83.3°E) covers an area of 313,147 km² in the central and southern parts of the Indian subcontinent. The river originates at Nasik, in the Western Ghats at an elevation of 1600 m above mean sea level and has 25 tributaries. Pranahita, Indravati, Wardha,

Manjeera and Sabari are some of the major tributaries of the Godavari River. The drainage basin is comprised of Deccan trap basalts (48%), late Archaean/early Proterozoic granites (39%), Precambrian and Gondwana (105-302 Ma: Mukhopadhyay et al., 2010) sedimentary rocks (11%) and recent alluvial cover (2%) (Biksham and Subramanian, 1988; Meert et al., 2010).

2.2 Mahanadi Basin

The Mahanadi offshore basin is a well known petroliferous basin located along the east coast of India (Singh, 2008). Mahanadi Basin extends from Jagannathpur in the north to Chilka Lake in the south and further extends offshore into the Bay of Bengal (Fig. 1).

It is a passive pericratonic basin covering an area of $260,000 \text{ km}^2$ with water depth exceeding 3000 m (including deep offshore) (Singh, 2008). The Mahanadi offshore area represents a pull-apart basin that generally parallels the coast and contains a sedimentary section showing rapid seaward thickening (Jagannathan et al., 1983). The basin originated during the break-up of Gondwanaland in Late Jurassic time. The Mahanadi basin is believed to have been formed at one of the three fossil triple junctions identified along the east coast of India (Burke and Dewey, 1973). The basement configuration inferred from the bathymetry, magnetic and gravity modelling resembles a series of coast-parallel structural highs and depressions (Subrahmanyam et al., 2008). Tectonically, the basin extends from Damra-Wheeler lineament in the north to 85° E ridge in the south. In the west, the basin continues into the Hasdo-Mahanadi Gondwana graben (Mohapatra, 2006). The basement is covered by volcanic and sedimentary successions ranging in age from Cretaceous to Holocene. The Lower Cretaceous volcanic and intertrappeans are successively overlain by Paleocene sand/silt/clay, Eocene carbonate, Lower to Middle Miocene clay/silt/minor limestone and Pliocene to younger sand/silt/clay (Jagannathan et al., 1983; Singh, 2008).

The Mahanadi River basin is characterized by a tropical climate. The drainage basin ($19^{\circ}21' - 23^{\circ}35' \text{N}$, $80^{\circ}30' - 86^{\circ}50' \text{E}$) extends over an area of about $1.42 \times 10^5 \text{ km}^2$ and has a total length of 850 km (Rao, 1975). The important tributaries of the Mahanadi River are the Sheonath, Jonk, Hasdeo, Mand, Ib, Tel and Ong. Late Archaean and early Proterozoic granite batholiths, Tonalite - Trondjhemite Gneisses (TTGs), and chanockites and khondalites of the Eastern Ghats constitute 56% of the catchment area. Sedimentary rocks (limestone, shale and sandstone) of Gondwana age (Mukhopadhyay et al., 2010) and recent alluvium/ littoral deposits constitute 39% and 5% of the catchment area, respectively (Chakrapani and Subramanian, 1990; Meert et al., 2010). The sediment

erosion rate varies from 116 to 940 ton km⁻²y⁻¹. Total erosion load of the Mahanadi basin is 5382.4 ton km⁻²y⁻¹.

3. Methodology

3.1 Coring and sub-sampling

The coring operation (NGHP-EXP1-3B, 5C and 18A) was carried out using conventional coring systems including the IODP's Advanced Piston Corer (APC) and the Extended Core Barrel (XCB). Both systems collect cores approximately 9.6 m long with a diameter of 6.7 cm. Transparent polycarbonate core liners were used for this purpose. Pressure coring systems (PCS) include Hyacinth Rotary Corer (HRC) and Fugro Pressure Corer (FPC). Each of these systems collects cores approximately 1 m in length with diameters of 5.7 cm (FPC), 5.1 cm (HRC) and 4.3 cm (PCS). Subsampling was carried out both as whole rounds at intervals of 1.5/ 6 m and also in one half of the longitudinally halved core (at high resolution) following IODP sampling protocol (Collett et al., 2008). NGHP-EXP1-3B and 5C were collected from the K-G basin and 18A from the Mahanadi basin.

The MD161-8 and 19 cores were collected on board the *Marion Dufresne* off K-G and Mahanadi basins, respectively. Cores were collected using a giant Calypso piston corer. Sampling locations are shown in Figure 1. PVC liners of 10 cm inner diameter were used for core collection (Mazumdar et al., 2012; 2014). Details of core locations are given in Table 1.

3.2 Geochemical analyses

Major oxide analyses were carried out following the fused pellet method and using a PANalytical X-ray Fluorescence Spectroscopy (XRF) Model Axios. Two grams of sediment were desalinated, dried and powdered. An aliquot (0.55 gm) of the moisture free sample was mixed with 5.5 gm of fusion mixture (A-100 Di-Lithium Tetra Borate with 0.07% Lithium Bromide) at a ratio of 1:10, homogenized, converted to melt at 1100°C in a platinum crucible and allowed to cool to become a glass bead. Accuracy of the data was assessed using an international standard reference material (JMS-1), and found to be better than ±3%.

Fifty mg of desalinated sediment sample was dissolved in 10 ml of ultrapure acid mixture (HF, HNO₃ and HClO₄) in a proportion of 7:3:1 in a PTFE beaker by heating on a hotplate. Additional acid mixture was added for complete dissolution. The semi-dry solution was redissolved in 4ml of

1:1 HNO₃ and subsequently diluted to 100 ml using ultrapure distilled water. International reference materials (SGR1 and SCO1) were digested following the above protocol. These solutions were analysed for trace and REE using an Inductively Coupled Plasma–Mass spectrometer (ICPMS Thermo X series- 2). The accuracy of the data was better than $\pm 6\%$.

Approximately 10 g of wet sediment was desalinated followed by removal of calcium carbonate by sodium acetate-acetic acid buffer. Suspensions were deflocculated with sodium hexametaphosphate and subsequently diluted to 1 litre in a measuring cylinder for separation of the <2 micron sized fraction (equivalent spherical diameter) following Stoke's law. An aliquot of each fraction was allowed to settle and dry on the glass slides. X-ray diffraction of the glycolated samples was carried out from 4 to 32° 2θ at 1°/min scan speed using CuK_α radiation ($\lambda = 1.5414\text{\AA}$) in a Rigaku X-Ray Diffractometer. Peak area relative quantification of clay minerals was carried out following Biscay (1965).

4. Results

4.1 Clay mineralogy

Illite contents in MD161-08 (Table 2) and MD161-19 (Table 3) range from 8 to 22% (avg: 15%) and 23 to 64% (avg.: 37%) respectively, whereas smectite contents in MD161-08 and MD161-19 range from 48 to 77% (avg.: 62%) and from 9.6 to 53.6% (avg.: 39%) respectively. The full width at half maxima (FWHM) or Kubler index (KI: Frey, 1987) of illite in Mahanadi samples ranges from 0.185 to 0.467 $\Delta^2\theta$ (avg.: 0.23 $\Delta^2\theta$). The smectite and illite contents show negative correlation in both MD161-8 and 19 (Fig. 2). The kaolinite + chlorite content in K-G and Mahanadi basin samples ranges from 12 to 33% (avg: 24%) and from 10 to 39% (avg: 25%) respectively. The triangular plot of kaolinite + chlorite, illite and smectite contents is given in figure 3. The triangular diagram shows significantly greater scatter of data points for the Mahanadi sediments compared with the K-G sediments.

4.2 Major element-oxide composition

The chemical compositions of the K-G basin sediments (NGHP-3B and 5C) are presented in Tables 4 and 5, and of Mahanadi basin sediments (NGHP-18A) in Table 6. Average compositions of the upper crust (Rudnick and Gao, 2003), post-Archean Australian average Shale (Taylor and McLennan, 1985), Deccan basalts (Pattanayak and Srivastava, 1999; Sano et al., 2001; Shukla and

Bhandari, 2001; Melluso et al., 2004) and the late Archaean-early Proterozoic granitic complex (Moyen et al., 2003) have been plotted in figures 4-7.

The average SiO₂ wt% concentrations in the K-G and Mahanadi basin sediments are 49.2 and 54.5, respectively. The plot of SiO₂ vs K₂O/Al₂O₃ ratios shows two clusters (Fig. 4A). The K-G sediments show lower average K₂O/Al₂O₃ ratios (0.13±0.01) and a broader range of SiO₂ (39-56 wt %) concentrations relative to the K₂O/Al₂O₃ (0.17) ratios and SiO₂ concentrations of the Mahanadi sediments. Except for two samples, the SiO₂ concentrations in the Mahanadi sediments range from 45.2- 58.4 wt%. The Fe₂O₃ concentrations range from 8.3-12.7 wt% (avg: 10.3 wt %) and from 5.4-10.7 wt% (avg: 7.2 wt %) in K-G and Mahanadi sediments, respectively. The Fe₂O₃ vs TiO₂ plot (Fig. 4B) defines two distinct fields for K-G and Mahanadi sediments. The TiO₂ concentrations for K-G and Mahanadi sediments are 0.88-1.95 wt% (avg: 1.3 wt %) and 0.6-1.0 wt% (avg: 0.9 wt %), respectively. The SiO₂ vs Fe/Al ratios define two separate fields for the K-G and Mahanadi sediments (Fig. 4C). The Fe/Al ratio in K-G sediments ranges from 0.6-1.07 (avg: 0.8), whereas in Mahanadi sediments, the Fe/Al ratio ranges from 0.4-0.73 (avg: 0.51).

4.3 Trace and REE variations

Rubidium concentrations in K-G and Mahanadi sediments range from 14-182.5 ppm (avg.: 105.9 ppm) and from 111.5-229.7 ppm (avg: 189 ppm), respectively (Fig. 4D). Uranium concentrations in the K-G and Mahanadi basin sediments range from 0.075-3.7 ppm and from 2.7-5.5 ppm, respectively. The Th concentrations are 15.8-45 ppm (barring one sample point with 2.8 ppm) for the K-G samples and 11.4-21.3 ppm for the Mahanadi samples. The Th/U ratio in the K-G and Mahanadi basins ranges from 13.1-48.3 and from 2.2-7.3, respectively (Figs. 5A, B). The La concentrations in K-G and Mahanadi basin sediments range from 4-57 ppm (avg: 35.3 ppm) and from 32-54 ppm (avg: 46.3 ppm) respectively. The Sc concentrations in K-G and Mahanadi basin sediments range from 2.6-31.8 (avg: 23.5 ppm) and 12.5-23.5 ppm (avg: 18.8 ppm), respectively. The average total REE concentrations in K-G and Mahanadi basin sediments are 188.8 ppm and 211.1 ppm, respectively (Fig. 7A, B). The average C1-chondrite normalized La/Yb ratio for the K-G sediments is 11.1 ppm and is 14 ppm for the Mahanadi basin sediments (Fig. 7C). Cerium and Eu anomalies were calculated using the formulas of Seto and Akagi (2008),

$$(Eu/Eu^*)_N = Eu_N / (Sm \times Gd)_N^{1/2} \quad (\text{Eq. 1})$$

$$(Ce/Ce^*)_N = Ce_N / (La \times Pr)_N^{1/2} \quad (\text{Eq. 2})$$

N stands for C1 chondrite normalized values. The Eu and Ce anomalies in the K-G basin sediments are 0.94-1.4 (avg: 1) and 0.7-0.9 (avg: 0.83), respectively. In the Mahanadi basin sediments Ce and Eu anomalies range from 1-1.2 (avg: 1.15) and 0.6-0.8 (avg: 0.69), respectively (Fig. 7D).

5. Discussion

5.1 Clay mineralogy

Relatively higher illite contents in the Mahanadi basin sediments compared to the K-G basin samples (Fig. 2) suggest a dominance of felsic source rocks, which characterize the Archaean-Proterozoic Gneissic Complex (APGC). Sixty eight percent of the KI values of illite in the Mahanadi sediments are within the anchizone limit of 0.42-0.25 $\Delta^2\theta$ (Kisch, 1990) whereas 32% of the KI values are below the higher anchizone limit of 0.25 $\Delta^2\theta$. This suggests significant contribution from rocks that have undergone incipient to epigenetic grade metamorphism (Blenkinsop, 1988). The highly crystalline illite recorded in the present study is not likely to be a result of diagenetic transformation of smectite to illite. Such transformation happens during burial diagenesis at significantly higher temperatures than what the sediments have experienced at a depth of 200 mbsf in the K-G and Mahanadi basins (Lanson et al., 2009; Pollastro, 1993). The bottom temperature at the coring locations is $\sim 6^\circ\text{C}$. The thermal gradient of $\sim 44^\circ\text{C}/1\text{km}$ results in a maximum burial temperature of $\sim 14^\circ\text{C}$ at a depth of 200 mbsf, which is insufficient for smectite to illite transformation.

High smectite contents in the K-G basin sediments indicate variable contributions from the Deccan basalts (Rao, 1991; Bhattacharyya et al., 1993; Salil et al., 1997; Das et al., 2005; Das and Krishnaswami, 2007). In the K-G basin drainage area, the Godavari River primarily drains the Upper Deccan basalt province whereas a significant portion of the Krishna drainage basin is composed of the Archaean-Proterozoic Dharwar granitic complex. The negative correlation observed between smectite and illite content may be attributed to the relative contribution of granitic and basaltic source rocks. The highly variable illite content in Mahanadi sediments (MD161-19) is responsible for the apparent scatter in the triangular plot (Fig. 3).

5.2. Sediment chemistry

The higher $\text{K}_2\text{O}/\text{Al}_2\text{O}_3$ ratios in the Mahanadi sediments relative to the K-G sediments suggest an important felsic contribution, which is related to a greater illite content. The Mahanadi data points plot closer to the composition of PAAS (Post-Archean Australian Shale; Taylor and McLennan,

1985), upper crust and APGC relative to the K-G basin data cluster, possibly due to a contribution from the Deccan basalt source (Fig. 4 A) to the K-G sediment composition.

The Fe_2O_3 vs TiO_2 diagram (Fig. 4B) defines two distinct areas for K-G and Mahanadi samples. The K-G field plots close to the average Deccan basalt composition whereas Mahanadi samples lie close to the average UCC (Upper Continental Crust: Taylor and McLennan, 1985; McLennan et al., 2006) and APGC compositions. However, mixing lines are not clear in this plot.

Considering that both Fe and Al are less mobile relative to K, Ca and Na and Mg during chemical weathering, the Fe/Al vs SiO_2 plot (Fig. 4 C) can be used as a provenance indicator. Total iron content (avg.: 7.2 wt %) in K-G basin sediments is significantly higher than the global average iron content of 3.69 and 4.29 wt% in continental margin and deep sea sediments, respectively (Poulton and Raiswell, 2002). The global average iron content of riverine sediments is 4.81wt% (Poulton and Raiswell, 2002). In contrast, the average Fe content in Mahanadi sediments is 5 wt% which is close to the global average of marine marginal sediments. The high iron content in the K-G basin sediments may be attributed to a contribution from the iron-rich mafic source rocks in the catchment area. The average total iron content of the Deccan basalts varies from ~9.1-11.2 wt% (Peng et al., 1998; Pattanayak and Shrivastava, 1999). Weathering of such iron-rich source rocks can produce iron-rich clay minerals, Fe-oxide and oxyhydroxide particulates and unaltered ferromagnesian siliciclastics (Das and Krishnaswami, 2007). The average Fe/Al ratio in the K-G sediments (0.87) falls in the middle of the mixing zone between Deccan basalts (1.2-1.6) and granites (0.2-0.48) of the K-G basin catchment area (Pattanayak and Shrivastava, 1999; Moyen 2003). The Fe/Al ratio (0.44-0.57) of Mahanadi basin sediments is close to the average Fe/Al ratio of the UCC. The average Fe/Al ratio of K-G basin sediments is close to the Fe/Al ratio (0.82) of clay fractions ($<2 \mu\text{m}$) (Peketi, 2012), suggesting that the clay fraction is the most important contributor of both Fe and Al in the sediments. The broad range of Fe/Al ratios in K-G basin sediments may be attributed to variable contributions from the Deccan basalts and granitic sources.

Rb-K

In sedimentary rocks, Rb is present mainly in K-feldspar, mica and clay minerals. Weathering of felsic rocks leads to a concentration of Rb relative to K owing to ion exchange and differential adsorption mechanisms (Heier and Billings 1970). The Rb^+ ion substitutes for K^+ in muscovite/illite and in the K-feldspar lattice. Rubidium shows low environmental mobility, mainly due to its very strong sorption by clay minerals such as illite (Dypvik and Harris, 2001). Because of its strong association with K, elevated Rb values in the weathered products may indicate a felsic provenance.

The K vs Rb plot (Fig. 4D) shows relatively higher Rb and K contents in the Mahanadi sediments compared to the K-G basin counterparts. Significantly higher Rb values in Mahanadi sediments relative to the UCC and APGC may be attributed to granitic source weathering, which tends to decrease K relative to Rb (Nesbitt et al., 1980; Wronkiewicz and Condie, 1987). The Rb content in the Mahanadi samples is close to the range observed in illite (Morton, 1985). Lower K and Rb in the K-G sediments are possibly due to the variable contributions from the Deccan province which is characterized by very low K and Rb concentrations.

U-Th and Th-Sc-La

The thorium-to-uranium ratios in sedimentary rocks range from < 0.02 to > 21 (Adams and Weaver, 1958). Most marine deposits have ratios much below 7. The plots displaying U vs Th concentrations and Th/U ratio vs SiO₂ concentrations (Fig. 5 A and B) show a marked difference in K-G and Mahanadi basin sediments. The K-G basin sediments are comparatively low in U and high in Th relative to the Mahanadi sediments (Fig. 5A). A high Th/U ratio (4-30) was reported by Rao (2010) from the Godavari clay formation of the K-G basin. The high Th/U ratio (Fig. 5B) observed in the K-G basin sediments may be attributed to the presence of monazite in variable amounts. Montel et al. (1996) reported a range of Th/U ratios (42-52) in monazites. Monazite-rich beach sands are known from the Waltair, Bimlipatnam, and Narasipatnam regions in the Krishna-Godavari coastal areas. In contrast, the average peninsular granite and gneisses (APGC) have Th/U ratios ranging from 1.9-7.2 (Rao et al., 1972). The high Th concentrations in cores 5C and 3B may be of local importance due to channels bringing in beach sand at the depositional sites. The Th/U ratios of the Mahanadi sediments (2.2-7.3) lie within the above range. The relatively high U in the Mahanadi sediments compared to the K-G basin may also be due to the presence of uranium-rich mineral deposits in or close to the Mahanadi drainage basin area. Uranium deposits are reported from the Proterozoic sedimentary rocks of Chattisgarh and Lower Gondwana in the Mahanadi graben (Sharma et al., 2011).

The La/Sc ratios can be used to discriminate felsic and mafic provenance (Taylor and McLennan, 1985). The La/Sc ratios of K-G and Mahanadi sediments range from 0.15-2.5 (avg.: 1.57) and 1.7-3.2 (2.4), respectively. The data clusters in the La-Th-Sc ternary diagram (Figs. 6A and B) fall between average basalt and granite, but closer to granite composition, suggesting a dominant contribution from the peninsular gneissic complex. The K-G basin data points show greater scatter, which is possibly due to a variable Deccan basalt derived component and monazite abundances.

Rare earth element distribution

All C1-chondrite normalised plots show LREE enrichment and negative Eu anomalies (Fig. 7A and B). The $(\text{La}/\text{Yb})_{\text{N}}$ ratios for Mahanadi basin sediments (avg: 14.6) are higher than those of the K-G basin sediments (avg: 11.2). The $(\text{La}/\text{Yb})_{\text{N}}$ ratios of the Deccan basalts range from 2- 5.1 (Melluso et al., 2004; Babechuk et al. 2013), which is markedly different from the $(\text{La}/\text{Yb})_{\text{N}}$ ratios (20-64.1) of the late Archaean-early Proterozoic continental gneissic and granitic complexes of the Dharwar craton (Moyen et al., 2003). High $(\text{La}/\text{Yb})_{\text{N}}$ ratios of 14-65 have also been reported from other Archaean granites (Smithies, 2000). The late Archaean granites and Tonalitic-Trondjemetic-Granodioritic complex (TTG) have $(\text{La}/\text{Yb})_{\text{N}}$ average ratios of 15.2-18.1 (Condie, 1993). Apparently, the Mahandi sediments have $(\text{La}/\text{Yb})_{\text{N}}$ ratios that reflect a mixture of Archaean granite- and TTG-derived products, whereas in the K-G basin sediments, the shift towards lower $(\text{La}/\text{Yb})_{\text{N}}$ ratios suggests a source contribution from the Deccan basalt.

On the Ce and Eu anomaly diagram (Fig. 7D), the K-G sediments have a consistently greater Eu anomaly than the Mahanadi sediments. The Eu anomaly is generally considered a feature derived from the sediment source (McLennan et al., 1993) due to very low mobility of Eu during weathering and post depositional diagenesis (Gao and Wedepohl, 1995). The Eu/Eu^* for the Mahanadi sediments are typical of a granitic contribution. The late Archaean peninsular granite and TTGs show a wide range of negative Eu anomalies between 0.48 and 1.0 (Condie, 1993; Gao and Wedepohl, 1995; Moyen et al., 2003), which makes it difficult to fix an end member composition. The chondrite normalized Eu and Ce anomaly values of PAAS are 0.65 and 1.05, respectively (Figure 7D). The relatively less pronounced Eu anomaly in K-G sediments is likely due to a contribution from the Deccan basalt, which does not show any chondrite normalized Eu anomaly (Alexander and Gibson 1977; Dessai et al., 2008; Babechuk et al., 2014). The spread in Eu anomaly values (Fig. 7D) suggests a variable source rock composition in the peninsular complex.

The positive Ce anomaly displayed by both the Mahanadi and K-G basin sediments could be a result of Ce mobilisation during diagenesis or during weathering of the parent rock(s). Cerium can undergo redox transformation from the insoluble Ce (IV) state (Ce-oxide) to soluble Ce (III) and vice-versa within the water column (De Baar et al., 1985) or at the sediment-water interface during early diagenesis (Sholkovitz et al., 1992). Coatings of organic matter and oxides of Mn and Fe on particle surfaces play a major role in the binding of Ce (IV). Due to its unique redox transformation under ambient oceanic conditions, variations in Ce anomalies have been used as a tracer for inferring paleoceanic redox conditions (Wright et al., 1987; Holser, 1997). Babechuk et al. (2014) have

determined both positive and negative anomalies in the weathered products of the Deccan basalts, including laterites. Such material can create positive cerium anomalies in the K-G basin sediments. In contrast, weathering of granitic rocks does not appear to result in any Ce anomalies in the weathering products (Cullers, 1988; Aubert et al., 2001). A significantly large range in Ce anomalies in the K-G sediments relative to the Mahanadi samples may be attributed to the contribution of weathered material derived from the Deccan basalts. Mobilization of Fe-Mn oxide associated Ce due to redox transformation at the sediment water interface may also result in Ce anomalies in sediment (Sholkovitz et al., 1992). Water column suboxia in the Bay of Bengal may also play a role in controlling the Ce anomaly in the sediments (Pattan et al., 2013).

6. Conclusion

Major element, trace element and REE composition, and clay mineralogy of clay-silt dominated sediments from two offshore basins (K-G and Mahanadi) along the western margin of the Bay of Bengal have been studied. The data set presented helps to carry out a systematic provenance analysis of K-G and Mahanadi offshore basin sediments.

Higher smectite contents in K-G basin sediments compared to the Mahanadi basin sediments suggests contribution from weathered products of the Deccan basalt. The $\text{SiO}_2\text{-K}_2\text{O}/\text{Al}_2\text{O}_3$, $\text{TiO}_2\text{-Fe}_2\text{O}_3$ and $\text{SiO}_2\text{-Fe/Al}$ plots show relatively greater scatter of data points for K-G sediments. The K-G basin data clusters fall closer to the average Deccan basalt data point suggesting a variable contribution of basalt-derived material in the K-G sediments compared with the primarily granitic-derived material in the Mahanadi sediments. The lower K and Rb in the K-G sediments supports this provenance interpretation. The Rb content in the Mahanadi sediments is close to the range observed in illite. Illite abundance and KI values within the epizonal to anchizonal range suggest a metamorphosed/crystalline source rock. The C1-chondrite normalized La/Yb ratios of the Mahanadi sediments fall close to the mixture of Archaean granites and TTG derived products. The negative Eu anomaly (0.48-1) of the Mahanadi sediments suggests a primarily granitic provenance whereas the insignificant Eu anomaly in the K-G sediments may reflect the variable contribution from the Deccan basalts.

The high Th/U ratio observed in the K-G basin sediments may be attributed to the presence of monazite in variable amounts. The high Th concentrations in cores 5C and 3B may be of local importance and result from channels transporting monazite beach sand to the depositional site. The positive Ce anomaly produced by the K-G sediments may be attributed to the contribution of

weathered material derived from the Deccan basalts, Ce dissolution and reprecipitation during early diagenesis, or water column suboxia in the Bay of Bengal.

Acknowledgment

We thank the director, CSIR-NIO for supporting this study and the MOES for providing funds for the acquisition of sediment cores and data. Sincere thanks are due to students of Goa University, IIT Kharagpur and project scientists of CSIR-NIO, NIOT, PRL and NGRI for the sampling activity on board MV Marion Dufresne. The NGHP coordinated by DGH is thanked for providing sediment samples of NGHP Gas Hydrate Expedition 01. G. Prabhu, M. Caesar and G. Parthiban for the help in availing XRD, XRF and ICP-MS facilities at NIO. Thanks to Daryl Vaz for preparing the geological map.

References

- Adams, J. A. S., and Weaver, C. E., 1958 Thorium-to-Uranium Ratios as Indicators of Sedimentary Processes: Example of Concept of Geochemical Facies. *AAPG Bull.* 42, 387-430.
- Alexander, P.O., Gibson, I.L., 1977. Rare earth abundances in Deccan trap basalts. *Lithos* 10, 143–147.
- Aubert, D., Stille, P., Probst, A., 2001. REE fractionation during granite weathering and removal by waters and suspended loads: Sr and Nd isotopic evidence. *Geochim. Cosmochim. Acta* 65, 387–406.
- Babechuk, M.G., Widdowson, M., Kamber, B.S., 2014. Quantifying chemical weathering intensity and trace element release from two contrasting basalt profiles, Deccan Traps, India. *Chem. Geol.* 363, 56–75.
- Bastia, R., 2007. Geologic Settings and Petroleum Systems of India's East Coast Offshore Basins: Concepts and Applications: Eastern Book Corporation, 204p.
- Berner, R. A., 1992. Weathering, plants, and the long-term carbon cycle. *Geochim. Cosmochim. Acta* 56, 3225–3231.
- Bhatia M. R. and Crook, K. A. W., 1986. Trace element characteristics of greywackes and tectonic setting discrimination of sedimentary basins. *Contribution Mineralogy Petrology*, 92, 181-193.
- Bhattacharyya, T., Pal, D. K., & Deshpande, S. B., 1993. Genesis and transformation of minerals in the formation of red (Alfisols) and black (Inceptisols and Vertisols) soils on Deccan basalt in the Western Ghats, India. *Journal of Soil Science*, 44, 159-171.
- Biksham, G., Subramanian, V., 1988. Sediment transport of the Godavari River basin and its controlling factors. *Journal of Hydrology* 101, 275-290.

- Biscaye, P. E. (1965) Mineralogy and sedimentation of recent deep-sea clay in the Atlantic Ocean and adjacent seas and oceans: *Geol. Soc. Am. Bull.* 76, 803-831.
- Blenkinsop, T.G., 1988. Definition of low-grade metamorphic zones using illite crystallinity, *Journal of Metamorphic Geology*, 6, 623–636
- Burke, K., Dewey, F.J., 1973. Plume generated triple junctions: key indicator in applying plate tectonic to old rocks. *J. Geology* 8, 406–439.
- Chakrapani, G. J., 1988. Nature of chemical and sediment load in the Mahanadi river basin. M. Phil. Dissertation, Jawaharlal Nehru University, New Delhi, 77 pp.
- Chakrapani, G. J., Subramanian, V., 1990. Preliminary studies on the geochemistry of the Mahanadi river basin, India. *Chem. Geol.* 81, 241-253.
- Collett, T., Riedel, M., Cochran, J., Boswell, R., Presley, J., Kumar, P., Sathe, A., Sethi, A., Lall, M., and Sibal, V., 2008. The NGHP Expedition 01 Scientists. Indian National Gas Hydrate Program Expedition 01 Initial Reports.
- Condie, K.C., 1993. Chemical composition and evolution of the upper continental crust: Contrasting results from surface samples and shales. *Chem. Geol.* 104, 1–37.
- Cullers, R. L. and Graf, J., 1983. Rare earth elements in igneous rocks of the continental crust: intermediate and silicic rocks, ore petrogenesis. *Rare-Earth Geochemistry* (Henderson, P., ed.), 275–312, Elsevier, Amsterdam.
- Cullers, R.L., Barrett, T., Carlson, R., Robinson, B., 1987. Rare earth element and mineralogic changes in Holocene soil and stream sediment: a case study in the Wet Mountains, Colorado, USA. *Chem. Geol.* 63, 275– 297.
- Cullers, R., 1988. Mineralogical and chemical changes of soil and stream sediment formed by intense weathering of the Danburg granite, Georgia, U.S.A. *Lithos* 21, 301–314.
- Cullers, R.L., 1994. The controls on the major and trace element variation of shales, siltstones, and sandstones of Pennsylvanian-Permian age from uplifted continental blocks in Colorado to platform sediment in Kansas, USA. *Geochim. Cosmochim. Acta* 58, 4955–4972.
- Cullers, R.L., 1995. The controls on the major- and trace-element evolution of shales, siltstones and sandstones of Ordovician to tertiary age in the Wet Mountains region, Colorado, U.S.A. *Chem. Geol.* 123, 107–131.
- Cullers, R.L., 2002. Implications of elemental concentrations for provenance, redox conditions, and metamorphic studies of shales and limestones near Pueblo, CO, USA. *Chem. Geol.* 191, 305–327.
- Das, A., Krishnaswami, S., Sarin, M.M., Pande, K.P., 2005. Chemical weathering in the Krishna Basin and Western Ghats of the Deccan Traps, India, *Geochim. Cosmochim. Acta* 69, 2067–2084.
- Das, A., Krishnaswami, S. 2007. Elemental geochemistry of river sediments from the Deccan Traps, India: Implications to sources of elements and their mobility during basalt–water interaction. *Chem. Geol.* 242, 232-254.

- Dasgupta, A.K., Ghose, A. and Chakraborty, K.K., 1993. Geological Map of India. Published by Geological Survey of India.
- De Baar, H.J.W., Bacon, M.P., Brewer, P.G., Bruland, K.W., 1985. Rare earth elements in the Pacific and the Atlantic oceans. *Geochim. Cosmochim. Acta* 49, 1943–1959.
- Dessai, A.G., Downes, H., López-Moro, F.-J., López-Plaza, M., 2008. Lower crustal contamination of Deccan Traps magmas: evidence from tholeiitic dykes and granulite xenoliths from western India. *Mineral. Petrol.* 93, 243–272.
- Dypvik, H., & Harris, N. B., 2001. Geochemical facies analysis of fine-grained siliciclastics using Th/U, Zr/Rb and (Zr+ Rb)/Sr ratios. *Chemical Geology*, 181, 131-146.
- Frey, M., 1987. Very low grade metamorphism in clastic sedimentary rock. In: M. Frey (ed.) Low temperature metamorphism, Blackie and sons Ltd. Glasgow, pp 9-58.
- Fralick, P. W., & Kronberg, B. I., 1997. Geochemical discrimination of clastic sedimentary rock sources. *Sedimentary Geology*, 113, 111-124.
- Gao, S., Wedepohl, K.H., 1995. The negative Eu anomaly in Archean sedimentary rocks: Implications for decomposition, age and importance of their granitic sources. *Earth Planet. Sci. Lett.* 133, 81–94.
- Gupta, S.K., 2006. Basin architecture and petroleum system of Krishna Godavari basin, east coast of India. *The Leading Edge* 25, 830.
- Haughton, P. D. W., Todd, S. P., & Morton, A. C., 1991. Sedimentary provenance studies. Geological Society, London, Special Publications, 57, 1-11.
- Heier, K.S., Billings, G.K., 1970. “Rubidium”. In: Wedepohl, K.H., (Ed.), *Handbook of geochemistry*. Springer, pp. 37-C-1-37-N-1.
- Holser, W.T., 1997. Evaluation of the application of rare-earth elements to paleoceanography. *Palaeo. Palaeo.* 132, 309–324.
- Hongxia, W., Xianjun, Z., Xianhong, L., Zhixun, Z., Zhenhong, L., Guangtao, Z., 2007. Geochemistry Characteristics of Sediment and Provenance Relations of Sediments in Core NT1 of the South Yellow Sea. *J. China Univ. Geosci.* 18, 287–298.
- Holser, W. T., 1997. Evaluation of the application of rare-earth elements to paleoceanography. *Palaeo. Palaeo.* 132, 309-323.
- Huang, W., Keller, W., 1970. Dissolution of rock-forming silicate minerals in organic acids: simulated first-stage weathering of fresh mineral surfaces. *Am. Mineral.* 55, 2076–2094.
- Jagannathan, C.R., Ratnam, C., Baishya, N.C., Das Gupta, U., 1983. Geology of the Offshore Mahanadi Basin. *Petrol. Asia J.* 6, 101-104.
- Kisch, H. J., 1990. Calibration of the anchizone: a critical comparison of illite 'crystallinity' scales used for definition. *Jour. Metamorphic Petrol.* 8, 31-46.

- Lanson, B., Sakharov, B., Claret, F. and Drits, V. A., 2009. Diagenetic smectite-to-illite transition in clay-rich sediments: A reappraisal of X-ray diffraction results using the multi-specimen method; *Am J Sci*, 309, 476-516.
- Mazumdar, A., Joao, H.M., Peketi, A. Dewangan, P., Kocherla, M., Joshi, R.K., Ramprasad, T., 2012. Geochemical and geological constraints on the composition of marine sediment pore fluid: Possible link to gas hydrate deposits. *Mar. Pet. Geol.* 38, 35-52.
- Mazumdar, A., Peketi, A., Joao, H.M., Dewangan, P., Ramprasad, T., 2014. Pore-water chemistry of sediment cores off Mahanadi Basin, Bay of Bengal: Possible link to deep seated methane hydrate deposit. *Mar. Pet. Geol.*, 49, 162-175.
- McLennan, S. M., 1989. Rare earth elements in sedimentary rocks; influence of provenance and sedimentary processes. *Reviews in Mineralogy and Geochemistry*, 21, 169-200.
- McLennan, S. M., Hemming, S., McDaniel, D. K., & Hanson, G. N., 1993. Geochemical approaches to sedimentation, provenance, and tectonics. *Special Papers-Geological Society of America*, 21-21.
- McLennan, S. M., 2001. Relationships between the trace element composition of sedimentary rocks and upper continental crust. *Geochem.Geophys. Geosys.* 2, 2000GC000109.
- Meert, J. G., Pandit, M. K., Pradhan, V. R., Banks, J., Sirianni, R., Stroud, M. Gifford, J. 2010. Precambrian crustal evolution of Peninsular India: A3.0 billion year odyssey. *J. Asian Earth Sci.*, 39, 483-515.
- Melluso, L., Barbieri, M., Beccaluva, L., 2004. Chemical evolution, petrogenesis, and regional chemical correlations of the flood basalt sequence in the central Deccan Traps, India. *J. Earth Syst. Sci.* 113, 587–603.
- Mohapatra, P., 2006. Sequence stratigraphic approach for Identification of hydrocarbon plays in Mahanadi offshore basin, 6th International Conference & Exposition on Petroleum Geophysics, pp.672-677.
- Montel, J. M., Foret, S., Veschambre, M., Nicollet, C., Provost, A., 1996. Electron microprobe dating of monazite. *Chem. Geol.* 131, 37-53.
- Morton, J. P., 1985. Rb-Sr dating of diagenesis and source age of clays in Upper Devonian black shales of Texas. *Geological Society of America Bulletin*, 96, 1043-1049.
- Moyen, J. F., Martin, H., Jayananda, M., Auvray, B., 2003. Late Archaean granites: a typology based on the Dharwar Craton (India). *Precambrian Res.* 127, 103–123.J.-F
- Mukhopadhyay, G., Mukhopadhyay, S. K., Roychowdhury, M., & Parui, P. K., 2010. Stratigraphic correlation between different Gondwana basins of India. *Journal of the Geological Society of India*, 76, 251-266.
- Nath, B.N., Kunzendorf, H., Plüger, W.L., 2000. Influence of provenance, weathering, and sedimentary processes on the elemental ratios of the fine-grained fraction of the bedload sediments from the Vembanad lake and the adjoining continental shelf, southwest coast of India. *J. Sediment. Res.* 70, 1081–1094.

- Nesbitt, H., Markovics, G. and Price, R. C., 1980. Chemical processes affecting alkalies and alkaline earths during continental weathering: *Geochim. Cosmochim. Acta* 44, 1659-1666.
- Nesbitt, H., Young, G., 1989. Formation and diagenesis of weathering profiles. *J. Geol.* 97, 129–147.
- Pattan, J.N., Mir, I.A., Parthiban, G., Karapurkar, S.G., Matta, V.M., Naidu, P.D., Naqvi, S.W.A., 2013. Coupling between suboxic condition in sediments of the western Bay of Bengal and southwest monsoon intensification: A geochemical study. *Chem. Geol.* 343, 55–66.
- Pattanayak, S. K., Shrivastava, J. P., 1999. Petrography and major-oxide geochemistry of Basalts from the eastern Deccan Volcanic province, India. In: Subbarao, K.V. (Eds.), *Deccan Volcanic province, West Volume*, pp. 233-270.
- Peketi, A., 2012. Marine sedimentary Sulfur-Carbon-Iron systematics: A study from Krishna Godavari Basin, Bay of Bengal. *Unpublished PhD Thesis*, pp
- Peng, Z., Mahoney, J., Hooper, P., Macdougall, J., Krishnamurthy, P., 1998. Basalts of the northeastern Deccan Traps, India: isotopic and elemental geochemistry and relation to southwestern Deccan stratigraphy. *J. Geophys. Res.* 103, 29843-29865.
- Perri F., Critelli S., Mongelli G., Cullers R.L., 2011a. Sedimentary evolution of the Mesozoic continental redbeds using geochemical and mineralogical tools: the case of Upper Triassic to Lowermost Jurassic M.te di Gioiosa mudstones (Sicily, southern Italy). *Int. J. Earth Sci.*, 100, 1569-1587.
- Perri, F., Muto, F., Belviso, C., 2011b. Links between composition and provenance of Mesozoic siliciclastic sediments from Western Calabria (Southern Italy). *Ital. J. Geosci.*, 130, 318-329.
- Perri, F., Critelli, S., Dominici, R., Muto, F., Tripodi, V., Ceramicola, S., 2012. Provenance and accommodation pathways of late Quaternary sediments in the deep-water northern Ionian Basin, southern Italy. *Sed. Geol.*, 280, 244-259.
- Perri, F., Critelli, S., Martin-Algarra, A., Martín-Martin, M., Perrone, V., Mongelli, G., Zattin, M., 2013. Triassic redbeds in the Malaguide Complex (Betic Cordillera – Spain): petrography, geochemistry, and geodynamic implications. *Earth-Sci. Rev.*, 117, 1-28.
- Pollastro, R. M., 1993. Considerations and applications of the illite/smectite geothermometer in hydrocarbon-bearing rocks of Miocene to Mississippian age. *Clays and Clay Minerals*, 41, 119-119.
- Poulton, S., Raiswell, R., 2002. The low-temperature geochemical cycle of iron: from continental fluxes to marine sediment deposition. *American Journal of Science* 302, 774-805.
- Prabhakar, K.N., Zutshi, P.L., 1993. Evolution of southern part of Indian east coast basins. *J. Geol. Soc. India* 41, 215-230.
- Ramana, M.V., Nair, R.R., Sarma, K.V.L.N.S., Ramprasad, T., Krishna, K.S., Subrahmanyam, V., D'Cruz, M., Subrahmanyam, C., Paul, J., Subrahmanyam, A.S., Sekhar, D.V.C., 1994. Mesozoic anomalies in the Bay of Bengal. *Earth Planet. Sci. Lett.* 121, 469-475.
- Ramesh, R., Subramanian, V., 1988. Temporal, spatial and size variation in the sediment transport in the Krishna River basin, India. *Journal of Hydrology* 98, 53-65.

- Rao, V., Aswathanarayana, U., Qureshy, M., 1972. Trace element geochemistry of parts of the closepet granite, Mysore State, India. *Mineral. Mag.* 38, 678–686.
- Rao, K. L., 1975. *Indias Water Wealth Orient Longman*, New Delhi, p. 255.
- Rao, V.P., 1991. Clay mineral distribution in the continental shelf sediments from Krishna to Ganges river mouth, east coast of India. *Indian J. Mar. Sci.* 20, 7–12.
- Rao, G.N., Mani, K.S., 1993. A study on generation of abnormal pressures in Krishna-Godavari basin. *Indian J. Petrol. Geol.* 2, 20-30.
- Rao, G.N., 2001. Sedimentation, stratigraphy, and petroleum potential of Krishna-Godavari basin, east coast of India. *AAPG Bull.* 85, 1623-1643.
- Rao, A. B., 2010. Clay-typing, depositional environment and framing a petrophysical model for formation evaluation in Vashista field, Krishna-Godavari basin -a case study. 8th Biennial International Conference and Exposition on Petroleum Geophysics, P-62, 1-8.
- Ronov, A. B., Balashov, Y. A., Girin, Y. P., Bratishko, R., Kazakov, G. A., 1974. Regularities of rare-earth element distribution in the sedimentary shell and in the crust of the earth. *Sedimentology*, 21, 171-193.
- Roy, M., van de Flierdt, T., Hemming, S.R., Goldstein, S.L., 2007. $^{40}\text{Ar}/^{39}\text{Ar}$ ages of hornblende grains and bulk Sm/Nd isotopes of circum-Antarctic glacio-marine sediments: Implications for sediment provenance in the southern ocean. *Chem. Geol.* 244, 507–519.
- Rudnick, R., Gao, S., 2003. Composition of the continental crust. *Treatise on Geochemistry* 3, 1–64.
- Salil, M.S., Shrivastava, J.P., Pattanayak, S.K., 1997. Similarities in the mineralogical and geochemical attributes of detrital clays of Maastrichtian Lameta Beds and weathered Deccan basalt, Central India. *Chem. Geol.* 136, 25–32.
- Sastri, V. V., Sinha, R. N., Singh, G., Murti, K. V. S., 1973. Stratigraphy and tectonics of sedimentary basins on east coast of peninsular India. *AAPG Bulletin* 57, 655-678.
- Sano, T., Fujii, T., Deshmukh, S., 2001. Differentiation processes of Deccan Trap basalts: contribution from geochemistry and experimental petrology. *J. Petrol.* 42, 2175–2195.
- Seto, M and Akagi, T., 2008, Chemical condition for the appearance of a negative Ce anomaly in stream waters and groundwaters, *Geochemical Journal*, Vol. 42, pp. 371 to 380.
- Sharma, U. P. Bidwai, R Jain, .S. K. Roy, M. K. Sinha, P. K. Majumdar, A., 2011.Uranium mineralization in Talchir Formation of Gondwana, Supergroup, Surguja District, Chhattisgarh. *Current Sci.*, 100, 984-986.
- Sholkovitz, E.R., Shaw, T.J., Schneider, D.L., 1992. The geochemistry of seasonally anoxic water column and pore-water of Chesapeake Bay. *Geochim. Cosmochim. Acta* 56, 3389–3402.
- Shukla, A., Bhandari, N., 2001. Geochemistry and magnetostratigraphy of Deccan flows at Anjar, Kutch. *J. Earth Syst. Sci.* 110, 111–132.

- Singh, L., 2008. Mahanadi Basin (Mahanadi -NEC basin) Oil and gas fields of India, Indian Petroleum publishers, Dehradun, India. 325-346.
- Smithies, R. H., 2000. The Archaean tonalite–trondhjemite–granodiorite (TTG) series is not an analogue of Cenozoic adakite. *Earth Planet. Sci. Lett.* 182, 115–125.
- Subrahmanyam, V., Subrahmanyam, A.S., Murty, G.P.S., Murthy, K.S.R. 2008. Morphology and tectonics of Mahanadi Basin, northeastern continental margin of India from geophysical studies. *Mar. Geol.* 253, 63–72.
- Taylor, S. R., McLennan, S. M., 1985. The continental crust: its composition and evolution. Oxford, Blackwell, 312 p.
- Wei, G., Liu, Y., Li, X., Shao, L., Liang, X., 2003. Climatic impact on Al, K, Sc and Ti in marine sediments: Evidence from ODP Site 1144, South China Sea. *Geochem. J.* 37, 593–602.
- Wei, G., Liu, Y., Li, X., Shao, L., Fang, D., 2004. Major and trace element variations of the sediments at ODP Site 1144, South China Sea, during the last 230 ka and their paleoclimate implications. *Palaeogeogr. Palaeoclimatol. Palaeoecol.* 212, 331–342.
- Welch, S., Ullman, W., 1993. The effect of organic acids on plagioclase dissolution rates and stoichiometry. *Geochim. Cosmochim. Acta* 57, 2125–2136.
- Weltje, G., Eynatten, H. Von, 2004. Quantitative provenance analysis of sediments: review and outlook. *Sediment. Geol.* 171, 1–11.
- Whitmore, G. P., Crook, K. A., & Johnson, D. P., 2004. Grain size control of mineralogy and geochemistry in modern river sediment, New Guinea collision, Papua New Guinea. *Sedimentary Geology*, 171, 129-157.
- Wright, J., Schreder, H., Holser, W.T., 1987. Paleoredox variations in ancient oceans recorded by rare earth elements in fossil apatite. *Geochim. Cosmochim. Acta* 51, 631–644.
- Wronkiewicz, J., Condie, K. C., 1987. Geochemistry of Archean shales from the Witwatersrand Supergroup, South Africa: Source-area weathering and provenance. *Geochim. Cosmochim. Acta* 51, 240 1-24 16.
- Wronkiewicz . J., Condie, K. C. 1989. Geochemistry and provenance of sediments from the Pongola Supergroup, South Africa: Evidence for a 3.0 Ga-old continental craton. *Geochim. Cosmochim. Acta* 53, 1537-I 549.
- Young, G.M., Nesbitt, H.W., 1998. Processes Controlling the Distribution of Ti and Al in Weathering Profiles, Siliciclastic Sediments and Sedimentary Rocks. *SEPM J. Sediment. Res.* 68, 448–455.

Figure Captions:

Figure 1. Geological map of K-G and Mahanadi drainage basins and locations of the offshore sediment cores. Legend description: A = Gondwana sediments, B = Quaternary sediments, C = Mid-Late Proterozoic sediments, D = Archean charnockite and khondalite, E = Archean Proterozoic gneissic complex, F= Deccan basalt, G = Early Proterozoic granites, H= Archean-Proterozoic Singhbhum metamorphic complex. Modified after geological map published by Geological Survey of India (Dasgupta et al., 1993).

Figure 2. Variation in illite and smectite contents in cores MD161-8 and MD161-19.

Figure 3. Ternary diagram of kaolinite + chlorite, illite and smectite contents in K-G and Mahanadi basin sediments.

Figure 4. Relationships between A) SiO₂ concentration and K₂O/Al₂O₃ ratio, B) Fe₂O₃ and TiO₂ concentrations C) SiO₂ concentration and Fe/Al ratio, and D) Rb vs. K concentrations. PAAS= post-Archean Australian shale, UCC = upper continental crust, APGC = Archean Proterozoic gneissic complex, DCB = Deccan basalt (References cited in text). 3B and 5C (K-G basin core), 18A (Mahanadi core).

Figure 5. Relationships between A) Th vs. U concentrations and B) SiO₂ concentration and Th/U ratio. 3B and 5C (K-G basin core), 18A (Mahanadi core).

Figure 6. Ternary plot of La-Th-Sc of the K-G and Mahanadi basin sediments.

Figure 7. C1-Chondrite normalized REE distribution patterns in A) K-G and B) Mahanadi basin sediments; C. Histogram showing C1-Chondrite normalised La/Yb ratios; D. Relationship between C1-chondrite normalized Ce and Eu anomalies. PAAS = post-Archean Australian shale. 3B and 5C (K-G basin core), 18A (Mahanadi core). C1 Chondrite normalizing values are from Palm (1988).

Table Captions:

Table 1. Details of core locations and water depths.

Table 2. Clay mineralogy of MD161-8. Quantification was carried out using X-ray diffractometry.

Table 3. Clay mineralogy of MD161-19.

Table 4. Major, trace and rare earth element concentrations of NGHP-3B

Table 5. Major, trace and rare earth element concentrations of NGHP-5C

Table 6. Major, trace and rare earth element concentrations of NGHP-18A

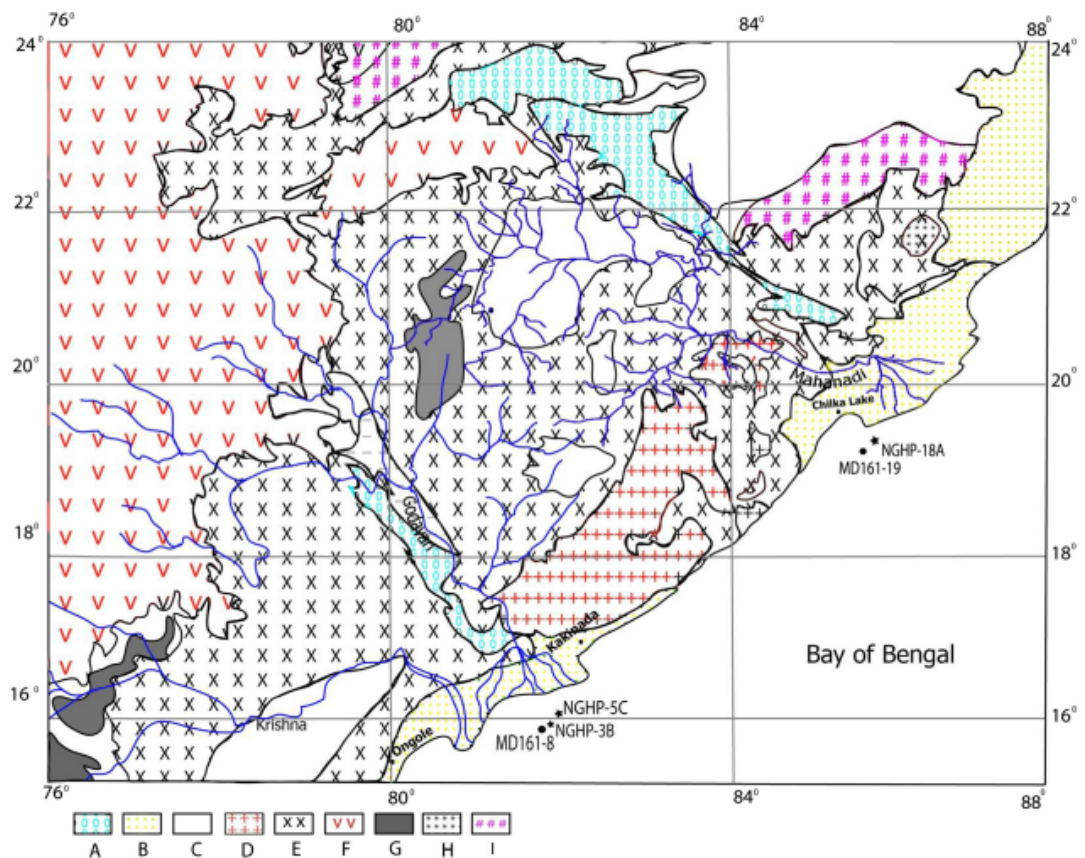


Figure-1

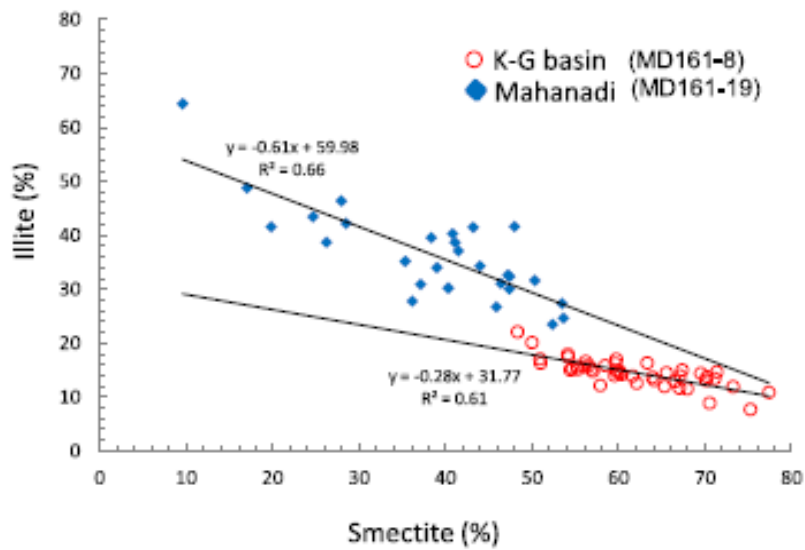


Figure-2

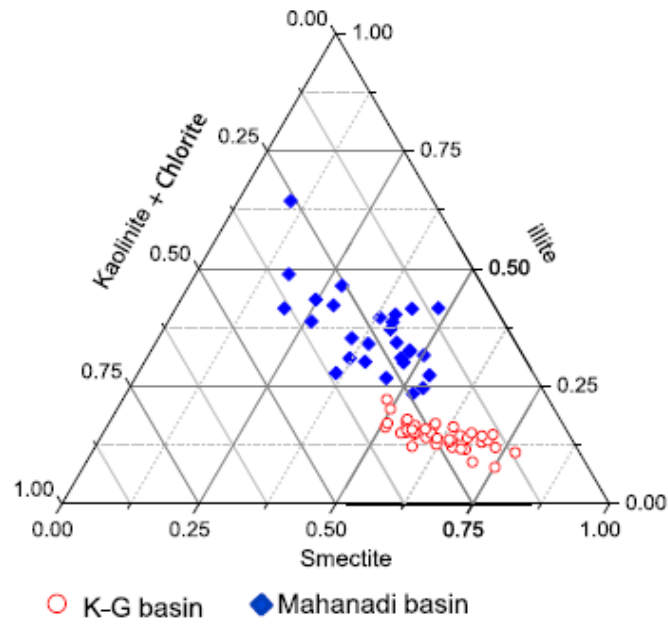


Figure-3

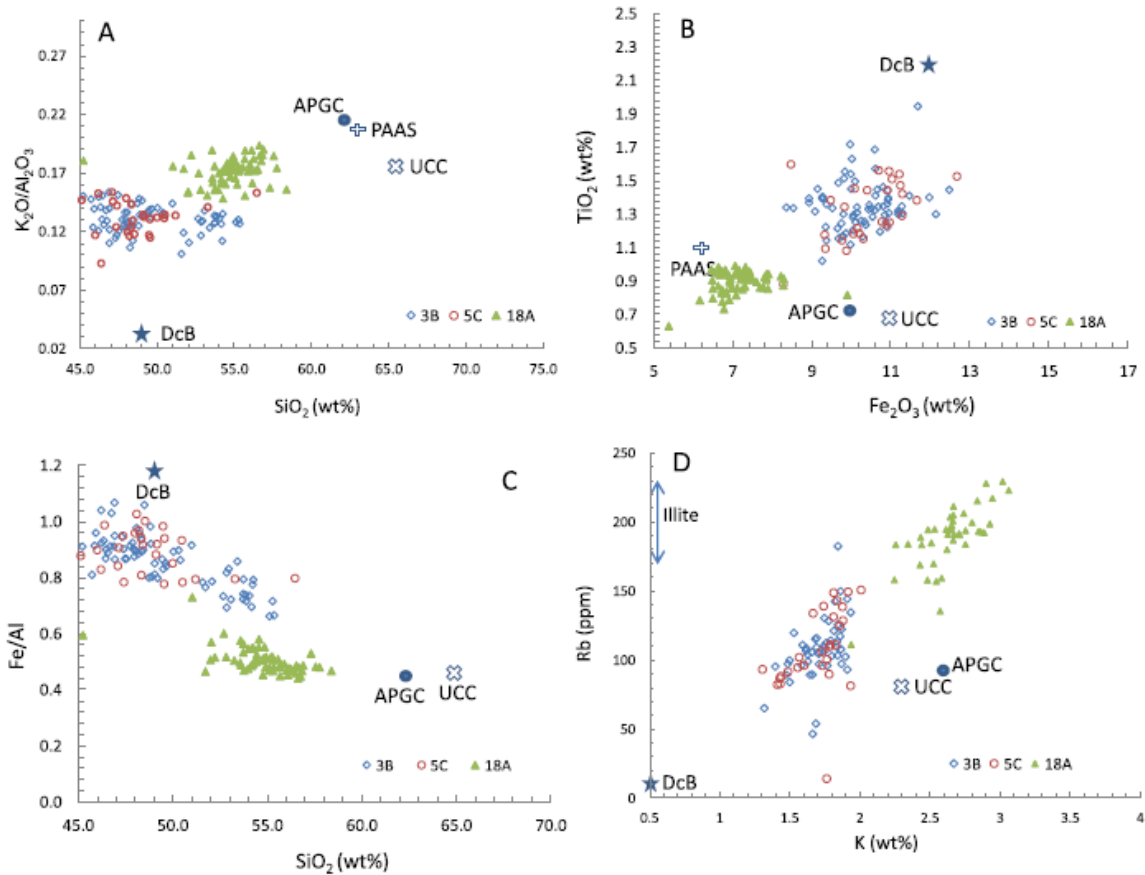


Figure-4

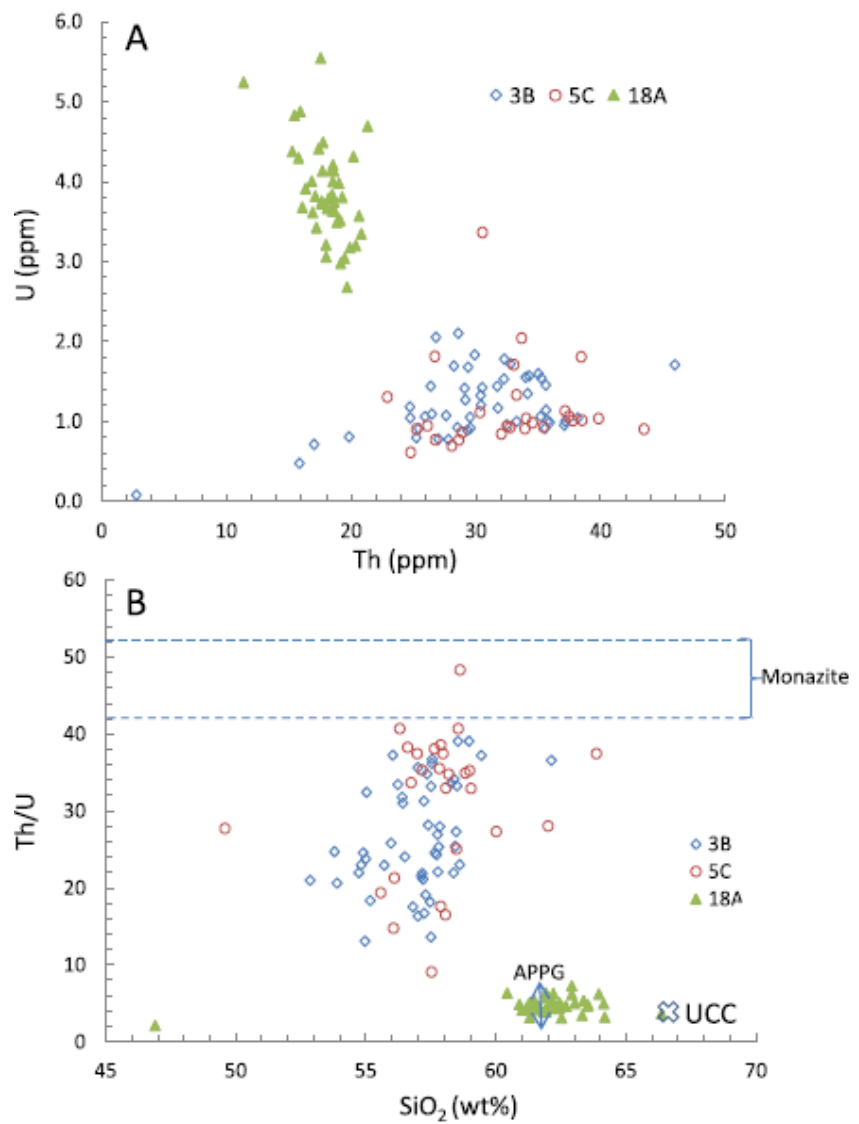


Figure-5

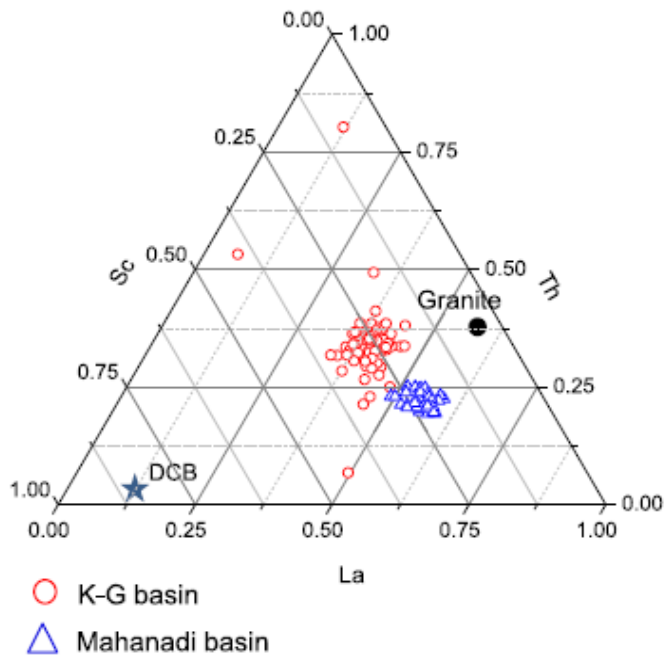


Figure-6

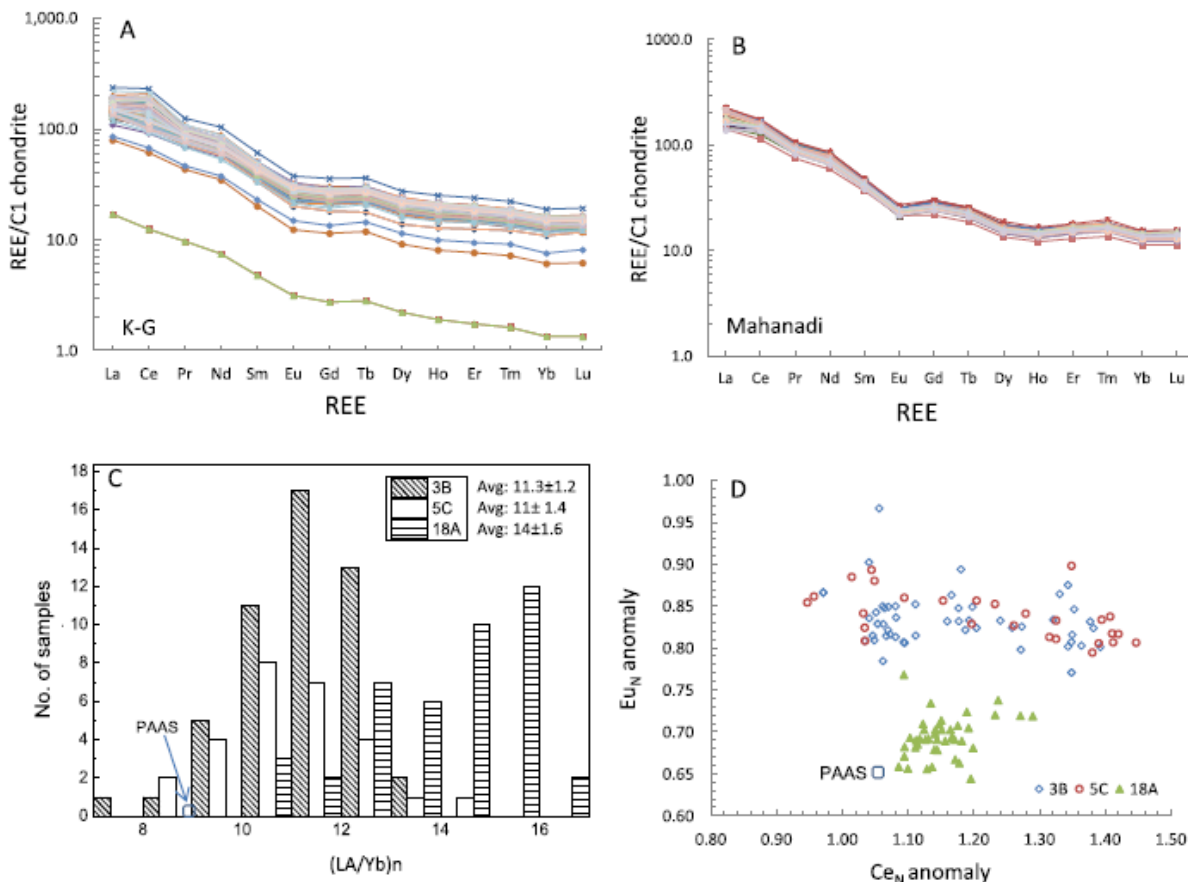


Figure-7

Table-1

Core Name	Latitude	Longitude	Water depth	Basin
MD161-8	15°51.864'	81°50.07'	1033	K-G
MD161-19	18°59.112'	85°41.166'	1480	Mahanadi
NGHP-EXP-1-3B	15°53.892'	81°53.97'	1076	K-G
NGHP-EXP-1-5C	16°01.722'	82°2.676'	945	K-G
NGHP-EXP-1-18A	19°09.144'	85°46.374'	1374	Mahanadi

Table-2

Depth (cmbfs)	Smectite (%)	Kaolinite +Chlorite (%)	Illite (%)	kaol+Chl/sm
43	60	25	14	0.4
104	66	21	13	0.3
135	68	21	12	0.3
209	60	26	15	0.4
250	77	12	11	0.2
321	57	28	15	0.5
375	55	30	15	0.5
421	60	25	15	0.4
521	62	25	13	0.4
575	51	33	16	0.6
621	56	28	16	0.5
674	58	30	12	0.5
724	70	21	9	0.3
824	57	28	15	0.5
874	59	26	14	0.4
921	55	30	15	0.5
950	65	20	15	0.3
974	51	32	17	0.6
1001	54	31	15	0.6
1034	70	16	14	0.2
1070	60	24	16	0.4
1124	48	30	22	0.6
1224	60	25	15	0.4
1260	50	30	20	0.6
1375	58	26	16	0.4

1424	75	17	8	0.2
1475	54	28	18	0.5
1524	65	23	12	0.3
1560	56	27	17	0.5
1625	64	23	13	0.4
1685	54	28	18	0.5
1785	55	29	16	0.5
1913	60	23	17	0.4
1955	56	28	16	0.5
2014	62	24	14	0.4
2123	67	21	12	0.3
2224	73	15	12	0.2
2260	63	20	16	0.3
2334	70	17	13	0.2
2415	67	19	14	0.3
2444	64	22	14	0.4
2510	71	15	14	0.2
2574	67	18	15	0.3
2714	71	14	15	0.2
2970	69	16	14	0.2
Min	48	12	8	0.2
Max	77	33	22	0.6
Average	62	24	15	0.4
Stdev	7	5	3	0.1

Table-3

Depth (cmbsf)	smectite (%)	Kaolinite +Chlorite (%)	illite (%)	Kaol+Chl/Sm
5	52	24	23	0.5
33	41	21	37	0.5
55	46	23	31	0.5
158	28	26	46	0.9
273	47	20	33	0.4
368	47	20	32	0.4
453	17	34	49	2.0
563	46	27	27	0.6
643	41	20	39	0.5
753	48	10	42	0.2
973	35	29	35	0.8
1053	40	29	30	0.7
1208	26	35	39	1.3
1368	37	32	31	0.9
1563	50	18	32	0.4
1733	20	39	42	2.0
1853	10	26	64	2.7
2073	36	36	28	1.0
2228	25	32	43	1.3
2418	28	29	42	1.0
2788	38	22	40	0.6
2833	41	19	40	0.5
3178	39	27	34	0.7
3323	54	22	25	0.4
3478	43	15	42	0.4
3628	47	23	30	0.5
3763	44	22	34	0.5
3888	53	19	27	0.4
Min	10	10	23	0.2
Max	54	39	64	2.7
Average	38	25	37	0.8
Stdev	11	7	9	0.6

Table-4

Depth (mbsf)	SiO ₂ (wt%)	Al ₂ O ₃ (wt%)	TiO ₂ (wt%)	Fe ₂ O ₃ (wt%)	MnO (wt%)	MgO (wt%)	CaO (wt%)	Na ₂ O (wt%)	K ₂ O (wt%)	P ₂ O ₅ (wt%)	Rb (ppm)	Sc (ppm)	Th (ppm)	U (ppm)
0	48.2	15.8	1.4	11.5	0.04	2.9	1.4	0.33	1.7	0.15	95.3		25.4	0.9
3	47.3	15.8	1.3	11.3	0.05	2.8	1.2	0.29	1.8	0.15	99.8	27.7	26.5	1.1
5.4	48.4	16.4	1.3	11.2	0.03	2.3	0.6	0.35	1.8	0.15	119.7	26.7	29.2	1.3
6.9	47.4	16.4	1.3	11.2	0.04	2.5	0.9	0.30	1.9	0.14	110.9	26.7	31.7	1.4
8.4	46.5	16.2	1.2	10.9	0.05	2.7	1.3	0.34	2.0	0.14	115.9	28.0	30.5	1.4
9.9	47.8	15.6	1.4	10.9	0.10	2.7	1.7	0.46	1.9	0.15	106.8	26.5	30.4	1.2
11.4	50.4	15.5	1.3	10.1	0.14	2.5	1.8	0.74	2.1	0.16	106.9	26.6	37.2	1.0
12.9	49.4	15.4	1.3	10.1	0.17	2.6	2.1	0.91	2.1	0.17	109.3	24.5	37.1	1.0
14.9	47.9	16.1	1.2	10.7	0.05	2.9	1.8	0.37	2.1	0.16	130.4	23.3	32.3	1.8
17.9	49.2	16.3	1.2	9.9	0.07	2.6	1.4	0.41	2.2	0.16	142.6	26.5	35.6	0.9
19.4	53.8	16.2	1.3	9.1	0.02	1.9	0.5	0.43	2.2	0.07				
23.9	49.0	15.9	1.2	9.8	0.08	2.8	2.2	0.46	2.3	0.15	134.5	22.3	31.8	1.2
27.4	55.1	17.0	1.3	8.5	0.03	1.9	0.6	0.50	2.2	0.09				
30.4	48.7	15.9	1.2	9.7	0.05	2.8	2.3	0.46	2.3	0.15	144.3	22.7	34.0	1.5
33.4	53.1	17.1	1.2	9.3	0.02	2.0	0.5	0.33	2.4	0.09				
35.4	44.6	14.4	1.0	9.3	0.04	2.9	6.2	0.45	2.2	0.15	114.1	24.7	26.8	2.1
39.9	46.2	14.8	1.2	10.4	0.10	3.0	3.4	0.66	2.2	0.15	109.4	22.1	33.3	1.0
42.9	53.7	16.9	1.4	9.3	0.03	2.3	0.6	0.53	2.3	0.08				
46.4	54.0	16.8	1.4	9.4	0.03	2.2	0.8	0.61	2.2	0.17				
49.4	46.7	14.0	1.4	10.9	0.14	3.1	3.8	0.83	1.8	0.17	83.9	22.9	25.3	0.8
51.9	53.9	17.1	1.4	9.3	0.03	2.3	0.6	0.54	2.3	0.11				
58.9	49.6	15.2	1.3	9.8	0.07	2.4	3.9	0.77	2.0	0.17	46.5	25.0	15.9	0.5
62.4	55.3	16.5	1.3	8.4	0.03	1.8	0.9	0.67	2.1	0.05				
66.9	46.7	14.8	1.3	10.2	0.08	3.1	3.5	0.87	2.1	0.16	105.3	10.2	28.5	0.9
68.7	55.3	16.4	1.4	8.9	0.03	1.9	1.0	0.69	2.1	0.11				
73.2	45.8	14.5	1.3	10.0	0.07	2.9	2.9	0.52	1.8	0.15	97.2	26.8	27.0	0.8
100.7	54.2	16.9	1.4	8.9	0.03	2.1	0.8	0.59	2.1	0.11	128.3	27.8	35.9	1.0

107.4	48.8	14.2	1.4	10.6	0.14	2.6	4.1	0.89	1.8	0.16	89.3	27.9	27.8	0.8
117	49.0	16.8	1.3	10.8	0.10	2.5	1.6	0.59	2.2	0.15	149.9	23.4	38.2	1.0
121.5	49.5	16.0	1.3	10.1	0.08	2.5	3.2	0.68	2.2	0.18	182.5	27.5	46.0	1.7
133.2	49.6	16.4	1.4	10.5	0.05	2.6	2.8	0.76	2.3	0.16	102.4	31.8	29.6	1.0
137.7	51.6	16.9	1.6	10.0	0.02	1.8	0.5	0.42	1.7	0.09				
141.9	46.9	16.0	1.3	10.5	0.03	2.5	2.7	0.57	1.9	0.14	108.6	24.2	29.4	1.7
151.7	50.0	15.8	1.3	10.7	0.06	2.4	2.2	0.69	2.2	0.15	113.4	23.9	34.2	1.3
156.2	48.1	16.0	1.3	10.9	0.05	2.6	2.3	0.53	2.2	0.15	121.2	23.3	34.3	1.6
157.96	54.2	16.9	1.7	10.0	0.03	1.8	0.7	0.56	1.9	0.07				
162.8	48.5	15.1	1.3	12.1	0.07	2.0	1.2	0.63	2.0	0.16	98.9	24.2	32.5	1.0
164.6	53.7	16.3	1.5	9.1	0.03	1.7	0.8	0.62	2.1	0.09				
167.6	47.5	17.0	1.3	11.2	0.07	2.3	1.1	0.56	2.1	0.18	97.1	22.2	35.8	1.0
175.5	48.3	15.9	1.3	11.3	0.08	2.3	1.8	0.57	2.0	0.17	105.7	24.1	35.6	1.5
178.99	52.1	16.7	1.5	10.0	0.02	1.7	0.7	0.45	1.9	0.08				
181.99	48.1	16.3	1.4	10.9	0.04	2.5	2.0	0.61	2.0	0.15	115.1	24.3	32.8	1.7
189.88	52.8	17.6	1.4	9.3	0.02	2.0	0.7	0.56	2.3	0.08				
192.88	48.9	17.1	1.3	10.4	0.04	2.5	1.6	0.65	2.3	0.15	93.1	26.2	29.3	0.9
193.16	45.9	14.2	1.3	10.3	0.08	3.4	5.5	0.65	2.0	0.19	89.3	26.7	24.8	1.0
197.8	51.7	16.7	1.5	9.7	0.02	1.9	0.8	0.56	2.0	0.09				
202.4	47.9	15.6	1.4	10.7	0.04	2.7	2.4	0.71	2.1	0.16	112.6	18.8	32.3	1.5
206.71	48.0	15.8	1.5	10.8	0.03	2.5	2.5	0.56	2.0	0.16	104.0	25.4	28.3	1.7
212.1	52.7	17.1	1.3	9.5	0.02	1.9	0.7	0.52	2.2	0.07				
216.3	46.4	15.6	1.2	10.3	0.03	2.6	2.7	0.42	2.0	0.14	109.2	24.9	29.9	1.8
220.3	52.8	15.9	1.6	9.8	0.02	1.9	0.8	0.54	1.9	0.08				
224.58	47.7	15.6	1.3	10.8	0.04	2.7	3.5	0.60	2.0	0.16	53.9	23.5	17.1	0.7
229.9	53.7	16.6	1.5	10.0	0.03	2.2	1.0	0.68	2.1	0.06				
232.7	46.9	15.2	1.4	10.9	0.06	3.0	3.2	0.78	2.1	0.17	14.0	18.1	2.8	0.1
235.7	48.1	16.2	1.4	12.0	0.08	2.9	2.4	0.63	2.1	0.18	104.6	2.7	27.6	1.1
241.08	47.5	14.7	1.2	9.6	0.05	3.2	5.8	0.78	2.2	0.19	125.5	26.9	35.3	1.5
245.46	46.4	14.7	1.2	10.0	0.06	3.2	6.0	0.65	2.2	0.20	103.3	26.9	30.4	1.3
251.6	54.2	16.3	1.5	9.8	0.04	2.5	1.2	0.77	2.2	0.13				

256.1	44.0	14.0	1.1	10.0	0.06	3.3	7.4	0.95	2.3	0.25	97.3	24.1	24.7	1.2
261.15	46.9	14.1	1.2	9.7	0.06	3.1	6.5	0.97	2.2	0.21	103.0	21.4	26.4	1.4
264.15	51.0	15.8	1.3	10.9	0.05	3.1	2.5	0.74	2.3	0.23				
267.7	45.2	14.2	1.2	9.8	0.06	3.2	7.4	0.65	2.1	0.19	95.9	21.6	29.1	1.4
272.2	53.4	16.3	1.7	10.6	0.04	2.5	1.1	0.69	2.0	0.11				
277.73	46.2	15.8	1.4	12.5	0.11	3.2	2.0	0.63	1.9	0.20	96.1	20.4	29.6	0.9
282.23	50.3	15.6	1.6	10.6	0.09	2.7	1.9	0.96	2.1	0.15	110.1	30.1	35.2	1.1
285.23	45.7	15.2	1.1	9.4	0.04	2.9	6.0	0.61	2.3	0.19	122.5	25.1	35.0	1.6
287.7	48.8	15.2	1.3	10.6	0.05	3.1	2.8	0.62	2.2	0.14	107.8	20.3	28.6	2.1
292.16	46.9	14.4	1.9	11.7	0.15	3.4	5.7	1.25	1.6	0.17	65.1	22.9	19.9	0.8
297.3	52.9	16.0	1.5	10.1	0.04	2.9	1.3	0.75	2.1	0.10				
301.8	46.3	14.2	1.3	10.0	0.08	3.5	6.0	0.78	2.0	0.19	89.5	23.4	25.9	1.1
Max	55.3	17.6	1.9	12.5	0.17	3.5	7.4	1.25	2.4	0.25	182.5	31.8	46.0	2.1
Min	44.0	14.0	1.0	8.4	0.02	1.7	0.5	0.29	1.6	0.05	14.0	2.7	2.8	0.1
Average	49.5	15.8	1.4	10.3	0.06	2.6	2.4	0.62	2.1	0.14	106.0	24.0	30.0	1.2
Stdev	3.0	0.9124	0.1476	0.8	0.03	0.5	1.8	0.18	0.2	0.04	25.8	4.6	6.6	0.4

Depth (mbsf)	La (ppm)	Ce (ppm)	Pr (ppm)	Nd (ppm)	Sm (ppm)	Eu (ppm)	Gd (ppm)	Tb (ppm)	Dy (ppm)	Ho (ppm)	Er (ppm)	Tm (ppm)	Yb (ppm)
0	31.2	61.6	6.7	27.0	5.2	1.2	3.9	0.7	3.6	0.7	2.1	0.3	1.9
3	29.4	66.6	6.6	28.1	5.8	1.4	4.8	0.9	4.9	1.0	2.8	0.4	2.3
5.4	31.1	72.3	6.9	29.4	6.1	1.5	4.9	0.9	5.0	1.0	2.8	0.4	2.3
6.9	34.5	83.4	7.5	31.0	6.3	1.5	5.1	1.0	5.0	1.0	2.8	0.4	2.3
8.4	34.2	71.0	7.4	31.3	6.1	1.5	4.9	0.9	4.8	1.0	2.7	0.4	2.2
9.9	34.5	76.5	7.2	30.8	5.9	1.5	4.8	0.9	4.8	0.9	2.7	0.4	2.2
11.4	36.4	81.4	7.9	32.9	6.6	1.7	5.4	1.0	5.4	1.1	3.1	0.5	2.5
12.9	42.3	104.9	8.8	37.0	7.1	1.7	5.7	1.0	5.3	1.1	3.0	0.4	2.4
14.9	42.2	105.9	8.6	37.8	7.1	1.7	5.6	1.1	5.4	1.1	3.0	0.4	2.4
17.9	35.0	74.7	7.6	31.5	6.4	1.5	5.0	0.9	4.8	1.0	2.8	0.4	2.3
19.4													
23.9	40.7	102.4	8.3	35.8	6.5	1.5	5.1	0.9	4.7	0.9	2.6	0.4	2.1

27.4													
30.4	35.5	91.7	7.5	31.9	5.9	1.4	4.7	0.9	4.3	0.9	2.4	0.3	2.0
33.4													
35.4	36.9	76.8	7.8	32.2	6.1	1.4	4.8	0.9	4.6	0.9	2.5	0.4	2.2
39.9	31.0	62.1	6.6	27.2	5.3	1.3	4.4	0.8	4.5	0.9	2.5	0.4	2.1
42.9													
46.4													
49.4	38.4	85.4	7.9	32.7	6.5	1.6	5.2	1.0	5.2	1.0	2.9	0.4	2.4
51.9													
58.9	33.6	67.8	7.4	30.6	6.4	1.7	5.4	1.0	5.5	1.1	3.1	0.5	2.5
62.4													
66.9	19.1	37.6	4.0	16.3	3.1	0.7	2.4	0.5	2.4	0.5	1.3	0.2	1.0
68.7													
73.2	38.2	86.9	8.0	34.3	6.9	1.7	5.5	1.1	5.4	1.1	3.2	0.5	2.5
100.7	35.3	79.6	7.6	30.5	6.4	1.6	5.2	1.0	5.1	1.0	2.8	0.4	2.2
107.4	45.3	116.1	9.2	38.5	7.4	1.8	5.9	1.1	5.9	1.2	3.3	0.5	2.7
117	37.7	84.4	8.0	32.9	6.5	1.7	5.4	1.0	5.5	1.1	3.0	0.5	2.5
121.5	48.6	126.0	9.9	41.7	7.8	1.9	6.4	1.2	6.1	1.2	3.5	0.5	2.8
133.2	57.0	142.0	11.4	49.0	9.5	2.2	7.6	1.4	7.1	1.5	4.1	0.6	3.2
137.7													
141.9	35.8	87.2	7.7	32.0	6.0	1.5	4.8	0.9	4.7	1.0	2.6	0.4	2.1
151.7	44.5	110.8	9.0	37.7	7.5	1.8	5.9	1.1	5.8	1.2	3.2	0.5	2.6
156.2	39.6	79.6	8.3	34.6	6.8	1.7	5.5	1.0	5.3	1.1	3.0	0.4	2.5
157.96													
162.8	38.3	78.0	8.3	34.2	6.6	1.7	5.4	1.0	5.4	1.1	3.0	0.5	2.5
164.6													
167.6	41.5	81.6	8.5	34.6	7.1	1.7	5.6	1.1	5.6	1.1	3.2	0.5	2.6
175.5	44.6	106.4	9.2	37.1	7.3	1.7	5.8	1.1	5.7	1.1	3.2	0.5	2.5
178.99													
181.99	43.1	99.6	8.8	37.1	7.2	1.8	6.1	1.2	6.0	1.2	3.4	0.5	2.7
189.88													

192.88	36.7	75.2	7.6	33.0	6.6	1.6	5.3	1.0	5.3	1.1	3.0	0.5	2.4	
193.16	26.4	56.3	6.3	26.3	6.3	1.9	5.5	1.1	5.7	1.1	3.3	0.5	2.5	
197.8														
202.4	34.8	68.5	7.0	29.3	5.5	1.3	4.5	0.8	4.4	0.9	2.4	0.4	2.0	
206.71	40.6	90.7	8.4	35.0	7.0	1.7	5.6	1.1	5.6	1.1	3.1	0.5	2.4	
212.1														
216.3	35.7	70.5	7.6	31.3	6.3	1.6	5.2	1.0	5.2	1.1	3.0	0.4	2.3	
220.3														
224.58	33.9	68.8	7.1	29.8	5.8	1.4	4.6	0.9	4.6	0.9	2.5	0.4	2.1	
229.9														
232.7	20.6	41.4	4.3	17.6	3.6	0.9	2.9	0.6	3.0	0.6	1.6	0.2	1.3	
235.7	4.1	7.6	0.9	3.5	0.7	0.2	0.6	0.1	0.6	0.1	0.3	0.0	0.2	
241.08	4.1	7.6	0.9	3.5	0.7	0.2	0.6	0.1	0.6	0.1	0.3	0.0	0.2	
245.46	43.7	111.4	9.4	38.9	7.8	2.0	6.2	1.2	6.2	1.3	3.5	0.5	2.8	
251.6														
256.1	36.5	74.2	7.8	32.7	6.8	1.6	5.5	1.0	5.6	1.1	3.3	0.5	2.6	
261.15	32.4	63.8	6.7	28.4	5.6	1.4	4.6	0.8	4.5	0.9	2.6	0.4	2.0	
264.15														
267.7	32.3	67.3	7.1	29.3	5.9	1.5	4.8	0.9	4.8	0.9	2.7	0.4	2.2	
272.2														
277.73	34.9	70.5	7.3	31.0	6.1	1.5	5.1	0.9	4.9	1.0	2.8	0.4	2.3	
282.23	38.1	98.3	8.3	34.3	7.3	1.9	6.1	1.2	6.3	1.2	3.4	0.5	2.7	
285.23	44.0	114.0	9.5	38.5	7.8	1.9	6.1	1.2	6.0	1.2	3.3	0.5	2.6	
287.7	37.8	97.9	7.8	32.6	6.3	1.5	4.9	0.9	4.7	1.0	2.7	0.4	2.2	
292.16	31.9	67.6	6.8	29.8	5.9	1.5	4.7	0.9	4.7	0.9	2.6	0.4	2.2	
297.3														
301.8	31.1	65.2	7.1	29.7	6.3	1.6	5.4	1.0	5.5	1.1	3.1	0.5	2.6	
Max	57.0	142.0	11.4	49.0	9.5	2.2	7.6	1.4	7.1	1.5	4.1	0.6	3.2	
Min	4.1	7.6	0.9	3.5	0.7	0.2	0.6	0.1	0.6	0.1	0.3	0.0	0.2	
Average	35.4	79.8	7.5	31.2	6.2	1.5	5.0	0.9	4.9	1.0	2.8	0.4	2.2	
Stdev	9.1	25.2	1.8	7.7	1.5	0.4	1.2	0.2	1.2	0.2	0.7	0.1	0.5	

Table-5

Depth (mbsf)	SiO ₂ (wt %)	Al ₂ O ₃ (wt %)	TiO ₂ (wt %)	Fe ₂ O ₃ (wt %)	MnO (wt %)	MgO (wt %)	CaO (wt %)	Na ₂ O (wt %)	K ₂ O (wt %)	P ₂ O ₅ (wt %)	Rb (ppm)	Sc (ppm)	Th (ppm)	U (ppm)
3.6	48.3	15.3	1.4	10.9	0.08	2.9	2.1	0.45	1.9	0.14	102.0	14.1	22.9	1.3
9.6	53.3	15.7	1.4	9.5	0.03	2.1	1.0	0.63	2.2	0.12	143.1	25.4	25.3	0.9
27.1	46.2	14.8	1.2	9.3	0.04	3.2	4.7	0.53	2.3	0.13	128.6	20.8	38.5	1.8
30.1	48.0	14.3	1.4	10.4	0.11	3.1	3.1	0.69	2.1	0.14	100.4	22.2	30.6	3.4
33.45	39.0	12.0	0.9	8.3	0.04	3.0	12.7	0.48	2.1	0.18	96.0	24.0	26.1	0.9
36.4	47.1	15.7	1.2	10.1	0.06	3.3	3.5	0.50	2.4	0.16	150.8	17.0	26.7	1.8
43.1	51.2	16.3	1.3	9.8	0.04	2.3	1.3	0.66	2.2	0.14	148.8	25.4	30.4	1.1
46.1	47.4	15.7	1.1	9.3	0.03	2.5	4.0	0.51	2.2	0.16	125.0	23.7	37.5	1.1
52.52	48.3	16.1	1.1	9.9	0.05	2.8	2.0	0.56	2.3	0.17	149.5	22.7	33.7	2.0
57.02	49.1	15.7	1.3	11.0	0.11	2.6	2.0	0.64	2.1	0.17	106.0	24.1	37.2	1.1
68.1	50.5	14.2	1.5	10.1	0.11	2.6	3.6	0.93	1.9	0.18	94.6	22.6	34.6	1.0
70.3	47.1	14.8	1.2	10.1	0.06	2.8	4.0	0.64	2.2	0.16	109.8	22.8	28.9	0.9
74.7	45.1	14.7	1.1	9.8	0.05	2.7	4.9	0.61	2.2	0.16	111.2	23.1	33.1	1.7
88	50.0	16.7	1.3	10.8	0.07	2.3	1.4	0.65	2.2	0.15	111.1	23.3	33.3	1.3
90.1	49.1	16.3	1.2	10.9	0.11	2.4	1.8	0.64	2.2	0.15	131.3	21.9	37.8	1.0
97.8	50.5	17.3	1.2	10.3	0.06	2.1	1.0	0.61	2.3	0.14	81.3	22.6	34.1	1.0
107.8	49.5	17.3	1.2	10.2	0.10	2.2	1.0	0.67	2.3	0.14	138.6	24.5	28.1	0.7
110.8	48.4	16.2	1.3	11.3	0.10	2.4	1.4	0.65	2.1	0.15	139.1	22.7	38.5	1.0
116.08	46.4	16.9	1.5	12.7	0.04	2.1	0.3	0.24	1.6	0.12	93.2	23.4	35.4	0.9
128.2	46.0	16.5	1.5	11.2	0.08	2.7	1.1	0.60	1.9	0.13	96.1	29.6	24.8	0.6
132.7	47.3	16.2	1.4	11.7	0.11	2.4	1.3	0.58	2.0	0.17	133.9	28.2	28.7	0.8
146.2	56.5	14.0	1.6	8.5	0.07	1.9	2.5	1.12	2.1	0.13	89.7	24.2	34.0	0.9
150.5	48.2	15.4	1.4	11.3	0.07	2.3	2.0	0.58	1.8	0.18	91.6	18.4	39.9	1.0
158.5	48.5	14.4	1.6	11.0	0.11	2.4	2.8	0.71	1.7	0.17	82.2	23.4	32.5	0.9
166.6	48.1	14.4	1.5	11.2	0.14	2.5	2.8	0.66	1.7	0.17	82.7	23.7	32.8	0.9
177.73	49.5	14.8	1.5	11.0	0.11	2.2	2.4	0.69	1.7	0.17	88.2	25.3	26.8	0.8
184.3	49.5	15.0	1.6	10.7	0.12	2.3	2.7	0.73	1.7	0.17	86.8	22.7	43.5	0.9

Max	56.5	17.3	1.6	12.7	0.14	3.3	12.7	1.12	2.4	0.18	150.8	29.6	43.5	3.4
Min	39.0	12.0	0.9	8.3	0.03	1.9	0.3	0.24	1.6	0.12	81.3	14.1	22.9	0.6
Average	48.4	15.4	1.3	10.4	0.08	2.5	2.7	0.63	2.1	0.15	111.5	23.0	32.4	1.2
Stdev	3.0	1.2	0.2	1.0	0.03	0.4	2.3	0.15	0.2	0.02	23.4	3.0	5.2	0.6

Depth (mbsf)	La	Ce	Pr	Nd	Sm	Eu	Gd	Tb	Dy	Ho	Er	Tm	Yb	Lu
	(ppm)													
3.6	31.2	61.6	6.7	27.0	5.2	1.2	3.9	0.7	3.6	0.7	2.1	0.3	1.9	0.3
9.6	32.0	67.6	7.0	29.9	6.3	1.6	5.1	1.0	5.3	1.1	2.9	0.4	2.4	0.3
27.1	40.6	112.5	8.8	35.8	6.9	1.6	5.3	1.0	5.0	1.0	2.8	0.4	2.3	0.3
30.1	34.1	81.2	7.5	30.8	6.3	1.6	5.0	0.9	5.0	1.0	2.9	0.4	2.3	0.3
33.45	34.7	77.0	7.6	31.5	6.7	1.7	5.5	1.1	5.7	1.1	3.2	0.5	2.5	0.4
36.4	28.6	57.2	6.3	25.1	5.2	1.3	4.1	0.8	4.2	0.9	2.4	0.4	2.0	0.3
43.1	38.2	75.1	8.1	33.0	6.7	1.7	5.6	1.1	5.5	1.1	3.1	0.4	2.5	0.4
46.1	46.0	119.9	9.1	39.6	7.6	1.8	6.0	1.1	5.8	1.2	3.2	0.5	2.6	0.4
52.52	36.6	88.0	7.8	31.9	6.1	1.5	4.8	0.9	4.7	0.9	2.7	0.4	2.2	0.3
57.02	43.9	117.4	9.3	38.1	7.3	1.8	5.8	1.1	5.7	1.1	3.1	0.5	2.6	0.4
68.1	41.5	111.3	8.9	36.0	7.3	1.8	5.8	1.1	6.0	1.2	3.4	0.5	2.6	0.4
70.3	36.8	74.2	8.1	32.8	6.9	1.8	5.7	1.1	5.9	1.2	3.3	0.5	2.7	0.4
74.7	36.1	88.6	7.8	32.7	6.7	1.7	5.5	1.0	5.5	1.1	3.1	0.5	2.5	0.4
88	39.0	89.4	8.3	34.3	6.9	1.7	5.6	1.0	5.6	1.1	3.1	0.4	2.5	0.4
90.1	44.5	116.2	8.9	37.9	7.4	1.8	5.9	1.1	5.7	1.1	3.3	0.5	2.6	0.4
97.8	44.6	115.5	9.0	37.8	7.3	1.8	5.9	1.1	5.9	1.2	3.4	0.5	2.8	0.4
107.8	37.7	94.1	7.9	33.0	6.9	1.7	5.7	1.0	5.4	1.1	3.0	0.4	2.4	0.3
110.8	53.1	131.3	10.0	41.3	7.8	1.8	6.2	1.1	5.9	1.2	3.3	0.5	2.6	0.4
116.08	44.7	115.9	9.1	38.0	7.4	1.8	6.0	1.1	5.7	1.2	3.4	0.5	2.7	0.4
128.2	32.8	58.9	7.0	28.4	6.6	1.7	5.6	1.1	5.8	1.2	3.4	0.5	2.7	0.4
132.7	33.3	61.7	7.3	29.2	6.4	1.7	5.5	1.1	5.7	1.1	3.1	0.5	2.7	0.4

146.2	43.5	108.6	9.1	37.2	7.2	1.8	6.1	1.1	5.9	1.2	3.4	0.5	2.7	0.4
150.5	46.4	113.4	9.4	38.6	7.0	1.7	5.8	1.0	5.2	1.1	2.9	0.4	2.4	0.3
158.5	37.0	84.2	7.9	32.2	6.7	1.7	5.5	1.0	5.5	1.1	3.1	0.5	2.5	0.4
166.6	36.4	71.3	8.0	32.2	6.6	1.8	5.6	1.0	5.6	1.1	3.1	0.5	2.5	0.4
177.73	36.0	73.6	8.0	32.1	7.0	1.8	5.9	1.1	6.1	1.2	3.3	0.5	2.6	0.4
184.3	39.6	101.5	8.4	33.5	7.0	1.9	5.8	1.1	5.9	1.2	3.3	0.5	2.7	0.4
Max	53.1	131.3	10.0	41.3	7.8	1.9	6.2	1.1	6.1	1.2	3.4	0.5	2.8	0.4
Min	28.6	57.2	6.3	25.1	5.2	1.2	3.9	0.7	3.6	0.7	2.1	0.3	1.9	0.3
Average	38.8	91.4	8.2	33.7	6.8	1.7	5.5	1.0	5.5	1.1	3.1	0.5	2.5	0.4
Stdev	5.6	22.2	0.9	4.0	0.6	0.2	0.5	0.1	0.6	0.1	0.3	0.0	0.2	0.0

Table-6

Depth (mbsf)	SiO ₂ (wt%)	Al ₂ O ₃ (wt%)	TiO ₂ (wt%)	Fe ₂ O ₃ (wt%)	MnO (wt%)	MgO (wt%)	CaO (wt%)	Na ₂ O (wt%)	K ₂ O (wt%)	P ₂ O ₅ (wt%)	Rb (ppm)	Sc (ppm)	Th (ppm)	U (ppm)
0.8	54.2	18.8	0.93	7.8	0.02	1.9	0.27	0.50	3.0	0.09	170.0	17.5	19.2	3.0
6.8	54.0	18.5	0.86	7.7	0.02	1.9	0.22	0.48	3.2	0.06	180.3	17.0	18.0	3.2
8.25	54.5	17.8	0.92	7.8	0.03	2.4	0.63	0.74	3.1	0.07	135.8	14.4	16.3	3.9
9.7	53.6	18.0	0.94	7.9	0.02	2.1	0.44	0.58	3.0	0.07	158.2	15.9	17.7	4.5
11.2	52.7	18.0	0.93	8.2	0.03	2.3	0.60	0.61	3.1	0.11	157.3	15.7	18.1	3.7
14.2	56.7	19.0	0.97	6.4	0.03	2.2	0.55	0.86	3.4	0.05	193.5	17.0	20.8	3.4
15.7	55.3	19.0	0.95	6.7	0.02	2.0	0.35	0.62	3.3	0.05	191.0	17.6	20.2	4.3
17.12	54.9	18.7	0.95	7.3	0.02	2.1	0.47	0.75	3.4	0.05	193.2	17.1	20.6	3.6
17.7	55.9	18.5	0.90	6.9	0.02	1.9	0.27	0.58	3.2	0.05	194.4	17.5	19.1	3.5
19.2	57.5	18.2	0.94	6.7	0.02	2.0	0.39	0.71	3.4	0.05	199.9	16.0	19.9	3.2
20.7	55.6	19.3	0.96	6.6	0.02	2.2	0.43	0.76	3.5	0.05	198.9	18.0	20.4	3.2
22.3	54.9	18.5	0.91	7.2	0.02	2.1	0.35	0.59	3.3	0.05	191.9	16.9	18.5	4.2
23.7	56.5	19.2	0.96	6.7	0.01	2.0	0.34	0.63	3.3	0.06	184.1	17.1	19.3	3.8
25.2	55.2	18.6	0.91	7.3	0.02	2.2	0.33	0.60	3.2	0.06	191.3	17.0	18.2	3.8
30.2	56.8	18.7	0.98	6.6	0.03	2.2	0.56	0.88	3.5	0.05	192.6	20.6	19.7	2.7
33.2	56.2	18.9	0.97	6.8	0.03	2.4	0.54	0.82	3.4	0.05				
39.73	51.0	17.9	0.82	9.9	0.02	2.1	0.32	0.53	3.1	0.05				
42.68	55.3	19.1	0.92	6.9	0.02	2.1	0.31	0.64	3.3	0.05	206.5	19.7	18.5	3.6
45.69	53.7	19.4	0.91	7.8	0.03	2.3	0.51	0.72	3.4	0.08				
47.62	54.1	19.4	0.97	7.2	0.02	2.1	0.37	0.60	3.2	0.05	187.1	20.3	18.9	3.5
50.62	52.2	18.5	0.85	7.2	0.03	2.3	0.42	0.67	3.4	0.07				
52.12	52.8	19.4	0.90	7.6	0.01	1.9	0.25	0.42	3.0	0.05	185.2	21.8	18.6	4.1
56.78	53.2	19.4	0.94	7.4	0.01	1.8	0.24	0.45	2.9	0.05	189.3	20.9	18.4	4.2
59.72	54.2	18.9	0.94	7.9	0.03	2.2	0.42	0.55	3.3	0.06				
61.15	54.7	19.1	0.95	7.3	0.02	2.0	0.31	0.57	3.2	0.05	203.9	21.7	19.0	4.0
63.45	54.8	19.1	0.93	7.4	0.03	2.2	0.50	0.71	3.5	0.05				
65.2	54.4	19.3	0.91	7.5	0.02	2.2	0.35	0.57	3.3	0.06	194.1	21.5	17.1	3.8

68.13	54.4	18.5	0.92	7.4	0.02	2.2	0.49	0.59	3.2	0.06				
69.63	56.3	18.6	0.95	6.6	0.02	1.9	0.34	0.66	3.2	0.05	201.2	22.6	18.5	3.8
72.64	56.9	18.9	0.86	7.0	0.02	2.3	0.32	0.65	3.6	0.05				
78.7	54.4	19.6	0.96	7.4	0.02	2.0	0.36	0.56	3.1	0.06	195.0	21.4	18.6	3.8
81.78	55.1	19.5	0.86	7.1	0.02	2.1	0.39	0.74	3.5	0.05	228.2	23.5	21.3	4.7
83.2	53.7	19.8	0.94	7.0	0.02	1.9	0.25	0.49	3.1	0.05				
91.2	55.3	19.4	0.91	7.5	0.02	2.1	0.34	0.62	3.4	0.06				
92.68	53.5	19.4	0.94	7.3	0.03	2.4	0.45	0.81	3.7	0.07	223.3	21.6	19.5	3.0

Depth (mbsf)	SiO ₂ (wt%)	Al ₂ O ₃ (wt%)	TiO ₂ (wt%)	Fe ₂ O ₃ (wt%)	MnO (wt%)	MgO (wt%)	CaO (wt%)	Na ₂ O (wt%)	K ₂ O (wt%)	P ₂ O ₅ (wt%)	Rb (ppm)	Sc (ppm)	Th (ppm)	U (ppm)
100.7	45.2	15.0	0.73	6.8	0.04	2.6	9.88	0.58	2.7	0.24				
102.2	37.8	13.6	0.63	5.4	0.05	3.2	16.94	0.43	2.3	0.24	111.5	12.5	11.4	5.3
105.18	55.5	18.7	0.93	7.2	0.03	2.5	0.60	0.73	3.3	0.05				
107.94	55.0	19.4	0.94	6.9	0.02	2.3	0.36	0.63	3.2	0.04	205.2	20.7	18.0	3.1
112.39	52.0	19.0	0.99	7.3	0.02	2.1	0.36	0.43	2.9	0.05	169.2	18.6	16.8	4.0
113.91	52.0	19.2	0.92	8.3	0.02	2.2	0.46	0.38	3.0	0.05				
116.7	51.7	18.3	0.91	6.5	0.02	2.0	0.37	0.60	3.2	0.05	196.2	20.6	17.4	4.4
124.22	55.2	18.6	0.87	7.3	0.02	2.2	0.34	0.52	3.0	0.05	194.7	18.5	16.9	3.6
124.26	54.7	19.8	0.97	6.8	0.02	2.2	0.40	0.62	3.3	0.05				
126.17	54.8	18.5	0.86	7.8	0.01	2.0	0.23	0.58	3.2	0.06	197.7	19.7	16.1	3.7
128.5	53.7	19.3	0.88	8.3	0.01	2.0	0.22	0.41	3.0	0.05				
130	53.9	19.6	0.99	7.1	0.02	2.1	0.32	0.50	3.1	0.05	195.1	19.0	18.5	4.0
135.97	53.6	19.2	0.96	7.1	0.02	2.5	0.48	0.49	3.1	0.07	159.6	18.1	15.4	4.8
138.31	54.5	18.8	0.86	7.9	0.02	2.3	0.36	0.70	3.4	0.05				
147.05	56.6	18.5	0.78	6.7	0.02	2.3	0.33	0.72	3.4	0.05				
155.6	54.1	19.6	0.94	7.2	0.02	2.1	0.36	0.53	3.2	0.05	191.5	19.0	17.7	4.1
158.6	57.3	17.6	0.82	7.1	0.01	1.9	0.22	0.44	2.8	0.05				
159.97	55.7	18.7	0.86	7.0	0.01	1.9	0.21	0.45	2.8	0.04	184.3	18.6	17.6	3.7
164.98	56.5	18.2	0.85	6.7	0.02	2.3	0.37	0.60	3.2	0.05				
165.83	57.7	18.4	0.83	6.7	0.02	2.2	0.28	0.61	3.2	0.04	211.7	19.0	17.2	3.4

169.72	56.0	19.2	0.83	6.8	0.02	2.3	0.33	0.62	3.4	0.05	215.7	19.6	17.5	5.6
176.03	56.1	18.2	0.86	6.5	0.01	2.0	0.29	0.54	2.9	0.04	183.8	19.2	15.9	4.9
178.57	56.1	19.3	0.87	6.6	0.02	2.2	0.34	0.68	3.3	0.04				
179.03	58.4	17.4	0.79	6.2	0.01	1.9	0.20	0.44	2.7	0.04	183.8	19.8	15.8	4.3
184.3	56.1	19.1	0.89	6.9	0.02	2.4	0.41	0.72	3.6	0.05	229.7	20.8	17.6	3.8
187.3	56.6	19.4	0.80	6.5	0.02	2.4	0.29	0.70	3.8	0.04				
188.8	55.7	19.0	0.79	6.9	0.02	2.3	0.29	0.59	3.6	0.05				
190.3	54.2	18.2	0.83	6.8	0.01	2.1	0.37	0.35	2.7	0.05	158.5	15.7	15.3	4.4
Max	58.4	19.8	0.99	9.9	0.05	3.2	16.94	0.88	3.8	0.24	229.7	23.5	21.3	5.6
Min	37.8	13.6	0.63	5.4	0.01	1.8	0.20	0.35	2.3	0.04	111.5	12.5	11.4	2.7
Average	54.5	18.7	0.90	7.2	0.02	2.2	0.78	0.60	3.2	0.06	189.3	18.8	18.0	3.9
Stdev	2.9	1.0	0.07	0.6	0.01	0.2	2.37	0.12	0.3	0.03	22.9	2.3	1.8	0.6

Depth (mbsf)	La (ppm)	Ce (ppm)	Pr (ppm)	Nd (ppm)	Sm (ppm)	Eu (ppm)	Gd (ppm)	Tb (ppm)	Dy (ppm)	Ho (ppm)	Er (ppm)	Tm (ppm)	Yb (ppm)	Lu
0.8	43.5	94.6	8.7	36.7	6.8	1.4	6.0	0.91	4.2	0.90	2.7	0.44	2.3	0.33
6.8	36.7	81.8	7.9	32.0	6.0	1.3	5.1	0.79	3.8	0.78	2.5	0.42	2.2	0.33
8.25	35.5	77.0	7.6	30.6	6.0	1.3	5.2	0.81	3.8	0.84	2.6	0.44	2.3	0.33
9.7	37.4	84.1	7.8	31.9	6.1	1.3	5.4	0.82	3.8	0.82	2.5	0.43	2.2	0.32
11.2	39.2	88.5	8.3	33.7	6.3	1.4	5.5	0.86	4.2	0.87	2.7	0.46	2.4	0.35
14.2	54.6	102.5	9.6	39.9	7.4	1.5	6.3	0.98	4.6	0.95	2.9	0.49	2.5	0.36
15.7	47.6	102.0	9.4	39.1	7.3	1.5	6.4	0.97	4.6	0.96	2.9	0.49	2.5	0.36
17.12	45.3	99.7	9.4	38.9	7.0	1.5	6.1	0.94	4.4	0.92	2.8	0.47	2.4	0.34
17.7	43.2	97.9	9.1	37.4	7.1	1.4	6.2	0.94	4.3	0.90	2.7	0.45	2.4	0.33
19.2	49.8	102.0	9.5	39.2	7.4	1.5	6.4	0.97	4.5	0.89	2.8	0.44	2.3	0.32
20.7	48.2	99.3	9.4	38.1	7.2	1.5	6.3	0.95	4.5	0.93	2.8	0.47	2.4	0.34
22.3	45.5	94.5	8.9	36.7	6.9	1.4	6.0	0.91	4.4	0.91	2.9	0.47	2.5	0.35
23.7	51.0	97.3	9.0	37.2	7.0	1.4	6.1	0.92	4.3	0.92	2.7	0.46	2.4	0.35
25.2	46.7	94.7	8.6	35.7	6.7	1.4	5.8	0.89	4.2	0.88	2.7	0.44	2.3	0.33

30.2	53.5	102.7	9.4	38.9	7.1	1.5	6.1	0.95	4.5	0.93	2.8	0.48	2.4	0.35
33.2														
39.73														
42.68	51.6	96.8	8.8	37.2	6.7	1.4	5.8	0.88	4.1	0.86	2.7	0.44	2.3	0.32
45.69														
47.62	54.2	104.4	9.3	38.5	7.1	1.5	6.2	0.96	4.5	0.95	3.0	0.49	2.6	0.37
50.62														
52.12	51.5	102.5	9.1	36.6	6.8	1.5	5.9	0.90	4.3	0.92	2.8	0.49	2.5	0.37
56.78	50.3	99.8	8.7	36.1	6.8	1.4	5.8	0.91	4.2	0.90	2.8	0.46	2.4	0.35
59.72														
61.15	52.5	101.5	9.3	38.3	7.1	1.5	6.1	0.93	4.4	0.93	2.7	0.46	2.4	0.34
63.45														
65.2	41.7	93.9	8.2	33.9	6.5	1.4	5.5	0.87	4.2	0.90	2.7	0.45	2.4	0.35
68.13														
69.63	52.5	100.3	9.1	37.7	7.1	1.5	5.9	0.92	4.3	0.90	2.7	0.45	2.4	0.34
72.64														
78.7	51.5	101.2	9.0	36.8	7.1	1.5	6.0	0.92	4.5	0.96	2.9	0.49	2.5	0.37
81.78	54.5	107.6	9.9	40.6	7.4	1.6	6.4	1.00	4.9	1.00	3.0	0.53	2.7	0.39
83.2														
91.2														
92.68	48.4	96.4	8.9	35.9	6.6	1.4	5.7	0.89	4.1	0.86	2.6	0.44	2.2	0.33

Depth (mbsf)	La (ppm)	Ce (ppm)	Pr (ppm)	Nd (ppm)	Sm (ppm)	Eu (ppm)	Gd (ppm)	Tb (ppm)	Dy (ppm)	Ho (ppm)	Er (ppm)	Tm (ppm)	Yb (ppm)	Lu
100.7														
102.2	34.2	69.1	6.9	27.9	5.6	1.3	4.6	0.72	3.5	0.73	2.2	0.37	1.9	0.28
105.18														
107.94	49.1	97.7	8.4	34.9	6.5	1.4	5.6	0.85	3.9	0.86	2.5	0.42	2.2	0.31
112.39	51.2	96.3	8.9	35.3	6.8	1.4	5.6	0.90	4.3	0.91	2.9	0.47	2.5	0.35
113.91														
116.7	51.7	101.3	8.8	36.9	6.7	1.4	5.8	0.89	4.2	0.90	2.8	0.47	2.4	0.35

124.22	50.0	97.6	8.5	35.9	6.6	1.4	5.6	0.86	4.0	0.85	2.6	0.43	2.3	0.32
124.26														
126.17	40.5	87.0	8.0	33.0	6.3	1.3	5.3	0.80	3.8	0.80	2.4	0.41	2.1	0.30
128.5														
130	51.9	100.1	9.0	37.4	6.7	1.4	5.7	0.94	4.4	0.90	2.9	0.49	2.5	0.37
135.97	41.0	88.9	8.1	32.8	6.2	1.3	5.3	0.84	4.0	0.82	2.7	0.45	2.4	0.35
138.31														
147.05														
155.6	49.5	97.9	8.7	35.4	6.7	1.4	5.8	0.91	4.2	0.90	2.8	0.46	2.4	0.35
158.6														
159.97	47.7	94.2	8.5	35.2	6.6	1.5	5.6	0.86	4.2	0.90	2.7	0.47	2.3	0.33
164.98														
165.83	51.5	96.4	8.9	35.8	6.8	1.4	5.7	0.88	4.1	0.87	2.6	0.43	2.2	0.33
169.72	44.0	92.0	8.3	33.5	6.5	1.4	5.5	0.88	4.1	0.89	2.8	0.47	2.5	0.37
176.03	34.0	84.6	7.7	31.4	6.1	1.3	5.2	0.82	3.9	0.82	2.6	0.44	2.3	0.34
178.57														
179.03	40.7	88.5	8.0	31.9	6.1	1.3	5.3	0.82	3.9	0.82	2.5	0.41	2.2	0.32
184.3	38.4	91.8	8.4	33.7	6.6	1.5	5.5	0.88	4.1	0.88	2.7	0.45	2.3	0.34
187.3														
188.8														
190.3	33.0	83.4	7.5	30.6	5.9	1.3	5.1	0.81	3.9	0.85	2.6	0.45	2.3	0.35
Max	54.6	107.6	9.9	40.6	7.4	1.6	6.4	1.00	4.9	1.00	3.0	0.53	2.7	0.39
Min	33.0	69.1	6.9	27.9	5.6	1.3	4.6	0.72	3.5	0.73	2.2	0.37	1.9	0.28
Average	46.3	94.9	8.7	35.6	6.7	1.4	5.7	0.89	4.2	0.88	2.7	0.45	2.3	0.34
Stdev	6.3	7.9	0.7	2.8	0.4	0.1	0.4	0.06	0.3	0.05	0.2	0.03	0.1	0.02